

AD-A093 687

DELAWARE UNIV NEWARK DEPT OF CIVIL ENGINEERING

F/S 8/3

A NUMERICAL MODEL FOR NEARSHORE CIRCULATION INCLUDING CONVECTIV--ETC(U)

JUL 79 B A EBERSOLE, R A DALRYMPLE

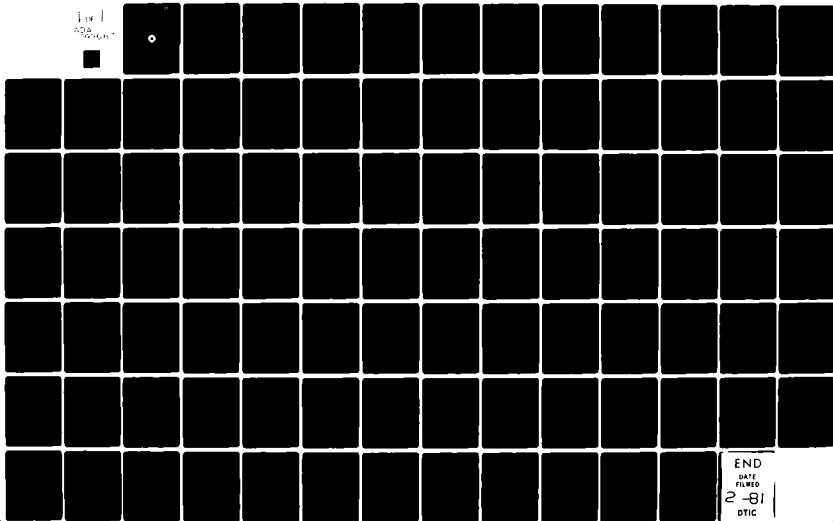
N00014-76-C-0342

OCEAN ENGINEERING-21

NL

UNCLASSIFIED

1 of 1
AD-A093 687



END
DATE
FILMED
2-81
DTIC

AD A093687

(2) LEVEL II YW

**A NUMERICAL MODEL FOR NEARSHORE CIRCULATION INCLUDING
CONVECTIVE ACCELERATIONS AND LATERAL MIXING.**

by
Bruce A. Ebersole
and
Robert A. Dalrymple



DTIC
ELECTE
S JAN 9 1981 D
B

(15) Technical Report No. 4
Contract No. N0014-76-C-0342
with the OFFICE OF NAVAL RESEARCH GEOGRAPHY PROGRAMS

(14) Ocean Engineering Report 21, TH-7

(11) July 1979

Department of Civil Engineering
University of Delaware
Newark, Delaware

DISTRIBUTION STATEMENT A
Approved for public release;
Distribution Unlimited

DDC FILE COPY

40-1595

A NUMERICAL MODEL FOR NEARSHORE CIRCULATION INCLUDING
CONVECTIVE ACCELERATIONS AND LATERAL MIXING

by

Bruce A. Ebersole

and

Robert A. Dalrymple

TECHNICAL REPORT NO. 4
OCEAN ENGINEERING REPORT NO. 21
Supported by ONR Contract Number *N00014-76-C-0342*
ONR Geography Programs

July, 1979

DISTRIBUTION STATEMENT A

Approved for public release;
Distribution Unlimited

TABLE OF CONTENTS

	<u>Page</u>
LIST OF FIGURES	ii
ABSTRACT	iv
CHAPTER I INTRODUCTION	1
CHAPTER II GOVERNING EQUATIONS	4
INTRODUCTION	4
BOUNDARY CONDITIONS	5
CONTINUITY EQUATION	6
MOMENTUM EQUATIONS	9
WAVE TRANSFORMATIONS INCLUDING WAVE-CURRENT INTERACTION	16
RADIATION STRESSES	21
WIND STRESS	22
BOTTOM STRESS	23
LATERAL MIXING	26
CHAPTER III FINITE DIFFERENCE FORMULATION	31
CHAPTER IV METHOD OF SOLUTION	42
CHAPTER V STABILITY ANALYSIS	48
CHAPTER VI RESULTS	51
PLANE BEACH APPLICATIONS	51
BARRED PROFILE APPLICATION	62
PERIODIC BOTTOM TOPOGRAPHY APPLICATION	64
INTERSECTING WAVES APPLICATION	70
CHAPTER VII CONCLUSIONS	81
APPENDIX A	83
APPENDIX B	84
REFERENCES	86

LIST OF FIGURES

<u>Figure</u>		<u>Page</u>
1	Planform Definition Sketch for the Wave Transformation Equations	19
2	Definition Sketch for the Bottom Friction Formulation	24
3	Longuet-Higgins' Analytical Solution for Oblique Wave Attack on a Plane Beach	27
4	Definition Sketch for the Lateral Mixing Formulation	28
5	Grid Scheme Definitions	32
6	Differencing Coordinate (i,j) Sketch	35
7	Initial Forward Difference and the First Leapfrog Solution Steps	46
8	General Leapfrog Solution Scheme	47
9	Plot of Inshore Mean Free Surface Displacement Versus Time for the Present Non-Linear Model Application to a Plane Beach	53
10	Plot of Offshore Mean Free Surface Displacement Versus Time for the Present Non-Linear Model Application to a Plane Beach	54
11	Plot of Inshore x-Velocity Component Versus Time for the Present Non-Linear Model Application to a Plane Beach	55
12	Plot of Inshore y-Velocity Component Versus Time for the Present Non-Linear Model Application to a Plane Beach	56

LIST OF FIGURES (CONTINUED)

<u>Figure</u>		<u>Page</u>
13	Longshore Current Profile for Plane Beach Case from Linear Model of Birkemeier and Dalrymple	58
14	Longshore Current Profile for Plane Beach Case from Present Model Excluding Mixing	60
15	Longshore Current Profile for Plane Beach Case from Present Model Including Mixing	61
16	Comparison of Barred Profile and Plane Beach	63
17	Longshore Current Profile for the Present Model Excluding Mixing Run on the Barred Profile	65
18	Longshore Current Profile for the Present Model Including Mixing Run on the Barred Profile	66
19	Current Vector Plot for the Model of Birkemeier and Dalrymple Run on the Periodic Bottom Topography	68
20	Current Vector Plot for the Present Model Including Mixing Run on the Periodic Bottom Topography	69
21	Definition Sketch for the Intersecting Waves Application	71
22	Current Vector Plot for a Rip Current Perpendicular to the Shoreline	77
23	Current Vector Plot for a Rip Current at an Angle to the Shoreline	79
24	Current Vector Plot for the Meandering Circulation Pattern	80

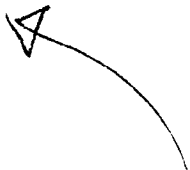
Accession For	
NTIS CR&I	<input checked="" type="checkbox"/>
DTIC TAB	<input type="checkbox"/>
Unannounced	<input type="checkbox"/>
Justification	
PER LETTER	
By	
Distribution/	
Availability Codes	
Dist	Avail and/or Special
A	



ABSTRACT

A finite difference model for predicting the nearshore circulation due to wind and waves is presented which attempts to solve the same problem as an earlier model created by Birkemeier and Dalrymple (1975). Their model iteratively solved the linear set of conservation equations of both mass and momentum, which were time averaged (over one wave period) and depth integrated, for mean velocities and free surface displacements. The wave characteristics used in the momentum equations were found using the wave refraction and shoaling routines, including wave-current interaction, developed by Noda, et al. (1974). The model also included a linear bottom friction formulation as well as a surface wind stress capability.

The present model discussed herein includes the addition of convective accelerations, horizontal mixing and a quadratic bottom friction term in the conservation of momentum equations. This bottom friction term is "exact" in the sense that it includes the velocity vectors due to both mean and wave-induced currents.



The model is applied to the cases of a single wave train impinging on a plane beach, a barred profile, and a bottom with a periodically spaced rip channel. It is also applied, in a simplified form, to the case of two intersecting wave trains at oblique angles to a plane beach. Results indicate that these additions to the model are important in attempts to model the circulation patterns over bottom bathymetries found in nature.

CHAPTER I INTRODUCTION

In recent years there has evolved a special interest in the environment around our extensive coastline. This interest is a result of the growing usage of these areas for industry and recreation. Those industries which rely on water as a primary mode of transportation for both raw materials and finished products are spending large amounts of time and money designing efficient access and docking facilities. Coastal communities are spending more money to maintain the condition of their recreational facilities located around water bodies. As people grow to depend on these regions for their livelihood, they become increasingly concerned with changes to the coastline and with efforts to maintain it in its present condition.

The problem of sediment transport is a primary concern of industry and resort communities. Its effects are clearly visible, yet an understanding of its causes and the ability to predict it accurately are just starting to unfold. An integral part of the sediment transport problem is an ability to describe the flows which serve to move sediment, such as the creation of a velocity field in the surf zone due to breaking waves.

Noda, et al. (1974) developed a steady state model which predicted the nearshore circulation due to waves and wind. Liu and Lennon (1978) also developed a steady state model using finite element techniques. Birkemeier and Dalrymple (1975), building on the efforts of Noda, et al., created a time dependent model to describe nearshore circulation due to the same forces. The effort reflected in this thesis is an attempt to extend the work of Birkemeier and Dalrymple one step further; to develop a more complete and accurate numerical model to predict flows along a coastline by including the effects of convective accelerations and lateral mixing, and by the use of a bottom friction term which includes the velocities due to both waves and mean currents.

There are many advantages to using a numerical model to investigate this problem. First of all, the problem at hand is so complex that only through numerical methods can it be solved. Secondly, the model enables the user to study an unscaled prototype situation. Thirdly, once the model has been established its generality enables it to be used theoretically on any stretch of beach. Finally, the model arrives at solutions rapidly when adapted to use with a high speed computer.

In order to formulate the problem so that it may be solved numerically the following requirements must be met:

- (1) a set of governing equations must be selected to accurately describe the physical processes at hand; the model is only as good as its governing equations,
- (2) boundary conditions must be established over the region of interest, and
- (3) initial conditions must be defined.

Only when these requirements are met can we hope to obtain an accurate solution.

CHAPTER II GOVERNING EQUATIONS

INTRODUCTION

The first step in problem formulation, as just mentioned, is the selection of governing equations that accurately describe the physical processes at work. This numerical model uses as its basis the equations describing conservation of both mass and momentum in a time averaged (over one wave period) and depth integrated form.

The purpose of the time averaging is to remove the fluctuations in time due to waves. The model deals only in mean quantities. The reasons for depth integrating the equations are, again, to deal with mean quantities, thus time over depth, and to reduce the problem from two horizontal and one vertical dimension into only two horizontal dimensions. In the process of depth integration the Leibnitz Rule was used to remove partial derivatives from within an integral. It is given by

$$\int_{\alpha(y)}^{\beta(y)} \frac{\partial f(x,y)}{\partial y} dx = \frac{\partial}{\partial y} \int_{\alpha(y)}^{\beta(y)} f(x,y) dx - f(\beta(y),y) \frac{\partial \beta(y)}{\partial y} + f(\alpha(y),y) \frac{\partial \alpha(y)}{\partial y}$$

The remainder of this chapter is devoted to the derivation of the integrated conservation of mass and momentum equations and the

"forcing" terms found in the momentum equations themselves. The three basic equations discussed above will be derived in detail. The equations which are solved to yield the wave characteristics, the radiation stresses, and the wind stress will be discussed briefly. For a more detailed derivation the reader is referred to the work of Noda, et al. and Birkemeier and Dalrymple. The bottom stress derivation and the formulation of the lateral mixing terms, however, will be discussed more fully as they are new additions to the model.

BOUNDARY CONDITIONS

Certain kinematic boundary conditions are used in the formulation of the mass and momentum equations. The boundary conditions state that if we move with a surface given by

$$F(x,y,z,t) = 0 \quad ,$$

then a water particle cannot flow across the surface, otherwise the surface would cease to exist. Mathematically, this condition is expressed by the total time rate of change of the function $F(x,y,z,t)$ equals zero.

$$\frac{D}{Dt} (F(x,y,z,t)) = 0$$

At the free surface the boundary is given by

$$F_1(x,y,z,t) = z - \eta(x,y,t) = 0$$

and at the bottom

$$F_2(x,y,z,t) = z + h(x,y,t) = 0$$

Therefore, for the kinematic free surface boundary condition (KFSBC),

$$\frac{\partial F}{\partial t} + u \frac{\partial F}{\partial x} + v \frac{\partial F}{\partial y} + w \frac{\partial F}{\partial z} = 0$$

or

$$w_\eta = \frac{\partial \eta}{\partial t} + u_\eta \frac{\partial \eta}{\partial x} + v_\eta \frac{\partial \eta}{\partial y} \quad (1)$$

For the bottom boundary condition (BBC) it can be shown that,

$$\frac{\partial \eta}{\partial t} + u_{-h} \frac{\partial h}{\partial x} + v_{-h} \frac{\partial h}{\partial y} + w_{-h} = 0 \quad (2)$$

where u, v, w are the velocity components in the x, y , and z directions and the subscripts denote the location of a specific term whether it be at the bottom, $z = -h$, or at the free surface, $z = \eta$.

CONTINUITY EQUATION

The general form of the three dimensional continuity equation which states that mass is conserved is,

$$\frac{\partial \rho}{\partial t} + \frac{\partial (\rho u)}{\partial x} + \frac{\partial (\rho v)}{\partial y} + \frac{\partial (\rho w)}{\partial z} = 0 \quad (3)$$

where ρ is the density of the fluid.

Integrating over depth from $z = -h(x, y, t)$ to $z = \eta(x, y, t)$ and using the Leibnitz Rule, Equation (3) becomes

$$\frac{\partial}{\partial t} \int_{-h}^{\eta} \rho \, dz - \rho_{\eta} \frac{\partial \eta}{\partial t} + \rho_{-h} \frac{\partial (-h)}{\partial t} + \frac{\partial}{\partial x} \int_{-h}^{\eta} \rho u \, dz$$

$$- \rho_{\eta} u_{\eta} \frac{\partial \eta}{\partial x} + \rho_{-h} u_{-h} \frac{\partial (-h)}{\partial x} + \frac{\partial}{\partial y} \int_{-h}^{\eta} \rho v \, dz$$

$$- \rho_{\eta} v_{\eta} \frac{\partial \eta}{\partial y} + \rho_{-h} v_{-h} \frac{\partial (-h)}{\partial y} + \rho_{\eta} w_{\eta} - \rho_{-h} w_{-h} = 0$$

Simplifying by substituting in both the KFSBC and the BBC, the continuity equation can be written

$$\frac{\partial}{\partial t} \int_{-h}^{\eta} \rho \, dz + \frac{\partial}{\partial x} \int_{-h}^{\eta} \rho u \, dz + \frac{\partial}{\partial y} \int_{-h}^{\eta} \rho v \, dz = 0 \quad (4)$$

Let both u and v be comprised of a time independent mean flow, a wave induced flow, and an arbitrarily fluctuating component (turbulence) such that

$$u = \bar{U} + \hat{u} + u'$$

$$v = \bar{V} + \hat{v} + v' .$$

It is important to note that the turbulent fluctuations u' and v' are of very high frequency and by definition their time averages (over a short period of time) are identically zero.

$$\frac{1}{T} \int_0^T u' dt \equiv 0$$

$$\frac{1}{T} \int_0^T v' dt \equiv 0$$

By substituting the above expressions for u and v into Equation (4), time averaging over one wave period so as to eliminate the wave induced fluctuations, and using the definitions for the time average of the turbulent components, the continuity equation can be written as

$$\begin{aligned} \frac{\partial}{\partial t} \{ \rho (h + \bar{\eta}) \} + \frac{\partial}{\partial x} \{ \rho \bar{U} (h + \bar{\eta}) \} + \frac{\partial}{\partial x} \overline{\int_{-h}^{\eta} \rho \hat{u} dz} \\ + \frac{\partial}{\partial y} \{ \rho \bar{V} (h + \bar{\eta}) \} + \frac{\partial}{\partial y} \overline{\int_{-h}^{\eta} \rho \hat{v} dz} = 0 \end{aligned} \quad (5)$$

where the symbol "—" denotes the time average over one wave period and $\bar{\eta}$ the time independent mean free surface displacement. Note that the time average of the vertically integrated wave induced velocities \hat{u} and \hat{v} is not zero.

Defining $U \equiv \bar{U} + \tilde{u}$

$$V \equiv \bar{V} + \tilde{v}$$

where $\tilde{u} = \frac{\overline{\int_{-h}^{\eta} \rho \hat{u} dz}}{\rho (h + \bar{\eta})}$ and $\tilde{v} = \frac{\overline{\int_{-h}^{\eta} \rho \hat{v} dz}}{\rho (h + \bar{\eta})}$

are the mass transport velocities and substituting the total depth D for $(h + \bar{\eta})$, the time averaged depth integrated continuity equation is, in its final form

$$\frac{\partial \bar{\eta}}{\partial t} + \frac{\partial}{\partial x} (UD) + \frac{\partial}{\partial y} (VD) = 0 \quad (6)$$

Also inherent in the derivation are the assumptions that the bottom is constant with time and the density is constant in space and time.

MOMENTUM EQUATIONS

The x and y momentum equations are manipulated in the same way as the continuity equation in order to achieve equations which are independent of wave induced oscillations, i.e., they are integrated over depth and time averaged over a wave period. The general form of the horizontal momentum equations are; in the x direction,

$$\frac{\partial u}{\partial t} + \frac{\partial u^2}{\partial x} + \frac{\partial uv}{\partial y} + \frac{\partial uw}{\partial z} = -\frac{1}{\rho} \frac{\partial P}{\partial x} + \frac{1}{\rho} \left\{ \frac{\partial \tau_{xx}}{\partial x} + \frac{\partial \tau_{yx}}{\partial y} + \frac{\partial \tau_{zx}}{\partial z} \right\} \quad (7)$$

and in the y direction,

$$\frac{\partial v}{\partial t} + \frac{\partial uv}{\partial x} + \frac{\partial v^2}{\partial y} + \frac{\partial vw}{\partial z} = -\frac{1}{\rho} \frac{\partial P}{\partial y} + \frac{1}{\rho} \left\{ \frac{\partial \tau_{xy}}{\partial x} + \frac{\partial \tau_{yy}}{\partial y} + \frac{\partial \tau_{zy}}{\partial z} \right\} \quad (8)$$

The x momentum equation will be dealt with first. Integrating the left hand side over depth and using the Leibnitz Rule to remove

derivatives from within the integra's give term by term,

$$(LHS) \int_{-h}^{\eta} \frac{\partial u}{\partial t} dz = \frac{\partial}{\partial t} \int_{-h}^{\eta} u dz - u_{\eta} \frac{\partial \eta}{\partial t} + u_{-h} \frac{\partial (-h)}{\partial t}$$

$$\int_{-h}^{\eta} \frac{\partial u^2}{\partial x} dz = \frac{\partial}{\partial x} \int_{-h}^{\eta} u^2 dz - u_{\eta}^2 \frac{\partial \eta}{\partial x} + u_{-h}^2 \frac{\partial (-h)}{\partial x}$$

$$\int_{-h}^{\eta} \frac{\partial uv}{\partial y} dz = \frac{\partial}{\partial y} \int_{-h}^{\eta} uv dz - u_{\eta} v_{\eta} \frac{\partial \eta}{\partial y} + u_{-h} v_{-h} \frac{\partial (-h)}{\partial y}$$

$$\int_{-h}^{\eta} \frac{\partial uw}{\partial z} dz = u_{\eta} w_{\eta} - u_{-h} w_{-h} .$$

Rearranging terms the (LHS) becomes,

$$\frac{\partial}{\partial t} \int_{-h}^{\eta} u dz + \frac{\partial}{\partial x} \int_{-h}^{\eta} u^2 dz + \frac{\partial}{\partial y} \int_{-h}^{\eta} uv dz$$

$$-u_{\eta} \left(\frac{\partial \eta}{\partial t} + u_{\eta} \frac{\partial \eta}{\partial x} + v_{\eta} \frac{\partial \eta}{\partial y} - w_{\eta} \right)$$

$$-u_{-h} \left(\frac{\partial h}{\partial t} + u_{-h} \frac{\partial h}{\partial x} + v_{-h} \frac{\partial h}{\partial y} + w_{-h} \right)$$

which after substituting the KFSBC and the BBC simplifies to,

$$(LHS) \quad \frac{\partial}{\partial t} \int_{-h}^{\eta} u dz + \frac{\partial}{\partial x} \int_{-h}^{\eta} u^2 dz + \frac{\partial}{\partial y} \int_{-h}^{\eta} uv dz .$$

Again letting the total velocities u and v be defined as

$$u = \bar{u} + \hat{u} + u'$$

$$v = \bar{v} + \hat{v} + v'$$

Substituting and averaging over a wave period, the (LHS) becomes term by term,

$$\frac{\partial}{\partial t} \overline{\int_{-h}^{\eta} u dz} = \frac{\partial}{\partial t} \overline{\int_{-h}^{\eta} \bar{u} dz} + \frac{\partial}{\partial t} \overline{\int_{-h}^{\eta} \hat{u} dz} + \frac{\partial}{\partial t} \overline{\int_{-h}^{\eta} u' dz}$$

$$\begin{aligned} \frac{\partial}{\partial x} \overline{\int_{-h}^{\eta} u^2 dz} &= \frac{\partial}{\partial x} \overline{\int_{-h}^{\eta} \bar{u}^2 dz} + \frac{\partial}{\partial x} \overline{\int_{-h}^{\eta} \hat{u}^2 dz} + \frac{\partial}{\partial x} \overline{\int_{-h}^{\eta} u'^2 dz} \\ &+ \frac{\partial}{\partial x} \overline{\int_{-h}^{\eta} 2\bar{u}\hat{u} dz} + \frac{\partial}{\partial x} \overline{\int_{-h}^{\eta} 2\bar{u}u' dz} + \frac{\partial}{\partial x} \overline{\int_{-h}^{\eta} 2\hat{u}u' dz} \end{aligned}$$

$$\begin{aligned} \frac{\partial}{\partial y} \overline{\int_{-h}^{\eta} u v dz} &= \frac{\partial}{\partial y} \overline{\int_{-h}^{\eta} \bar{u} \bar{v} dz} + \frac{\partial}{\partial y} \overline{\int_{-h}^{\eta} \bar{u} \hat{v} dz} + \frac{\partial}{\partial y} \overline{\int_{-h}^{\eta} \bar{u} v' dz} \\ &+ \frac{\partial}{\partial y} \overline{\int_{-h}^{\eta} \hat{u} \bar{v} dz} + \frac{\partial}{\partial y} \overline{\int_{-h}^{\eta} \hat{u} \hat{v} dz} + \frac{\partial}{\partial y} \overline{\int_{-h}^{\eta} \hat{u} v' dz} \\ &+ \frac{\partial}{\partial y} \overline{\int_{-h}^{\eta} u' \bar{v} dz} + \frac{\partial}{\partial y} \overline{\int_{-h}^{\eta} u' \hat{v} dz} + \frac{\partial}{\partial y} \overline{\int_{-h}^{\eta} u' v' dz} \end{aligned}$$

Since the frequency of the fluctuating components is much greater than the wave frequency, the wave induced velocity is essentially constant relative to the turbulent fluctuations. Therefore, integrals which involve products of a turbulent component and a wave induced component are zero in the time average. Using this result the (LHS) becomes,

$$\frac{\partial}{\partial t} \overline{\int_{-h}^{\eta} u dz} = \frac{\partial}{\partial t} \overline{\int_{-h}^{\eta} \bar{U} dz} + \frac{\partial}{\partial t} \overline{\int_{-h}^{\eta} \hat{u} dz}$$

$$\begin{aligned} \frac{\partial}{\partial x} \overline{\int_{-h}^{\eta} u^2 dz} &= \frac{\partial}{\partial x} \overline{\int_{-h}^{\eta} \bar{U}^2 dz} + \frac{\partial}{\partial x} \overline{\int_{-h}^{\eta} \hat{u}^2 dz} + \frac{\partial}{\partial x} \overline{\int_{-h}^{\eta} u'^2 dz} \\ &\quad + \frac{\partial}{\partial x} \overline{\int_{-h}^{\eta} 2\bar{U}\hat{u} dz} \end{aligned}$$

$$\begin{aligned} \frac{\partial}{\partial y} \overline{\int_{-h}^{\eta} uv dz} &= \frac{\partial}{\partial y} \overline{\int_{-h}^{\eta} \bar{U}\bar{V} dz} + \frac{\partial}{\partial y} \overline{\int_{-h}^{\eta} \bar{U}\hat{v} dz} + \frac{\partial}{\partial y} \overline{\int_{-h}^{\eta} \hat{u}\bar{V} dz} \\ &\quad + \frac{\partial}{\partial y} \overline{\int_{-h}^{\eta} \hat{u}\hat{v} dz} + \frac{\partial}{\partial y} \overline{\int_{-h}^{\eta} u'v' dz} . \end{aligned}$$

The right hand side after integrating over depth is

$$(RHS) \quad - \frac{1}{\rho} \int_{-h}^{\eta} \frac{\partial P}{\partial x} dz + \frac{1}{\rho} \int_{-h}^{\eta} \frac{\partial \tau_{xx}}{\partial x} dz + \frac{1}{\rho} \int_{-h}^{\eta} \frac{\partial \tau_{yx}}{\partial y} dz + \frac{1}{\rho} \int_{-h}^{\eta} \frac{\partial \tau_{zx}}{\partial z} dz ,$$

assuming the density is constant in space and time. If we also assume an inviscid fluid such that no horizontal viscous stress exists, then τ_{yx} and τ_{xx} become zero. Integrating over a wave period and invoking the Leibnitz Rule on the pressure gradient term, the (RHS) becomes,

$$-\frac{1}{\rho} \frac{\partial}{\partial x} \int_{-h}^{\eta} P dz + \frac{1}{\rho} \overline{P_{\eta}} \frac{\partial \eta}{\partial x} + \frac{1}{\rho} \overline{P_{-h}} \frac{\partial \eta}{\partial x} + \frac{1}{\rho} \overline{\tau_{zx_{\eta}}} - \frac{1}{\rho} \overline{\tau_{zx_{-h}}}$$

Assuming that the pressure at the free surface P_{η} is zero and realizing that $\overline{\tau_{zx_{\eta}}}$ and $\overline{\tau_{zx_{-h}}}$ are the time averaged surface and bottom shear stresses, the (RHS) is rewritten as

$$-\frac{1}{\rho} \frac{\partial}{\partial x} \int_{-h}^{\eta} P dz + \frac{1}{\rho} \overline{P_{-h}} \frac{\partial h}{\partial x} + \frac{1}{\rho} \overline{\tau_{sx}} - \frac{1}{\rho} \overline{\tau_{bx}}$$

The mean pressure at the bottom $\overline{P_{-h}}$ can be defined as the sum of the dynamic, or wave induced pressure at the bottom, and the hydrostatic pressure at the bottom such that

$$\overline{P_{-h}} = \overline{P_{dyn_{-h}}} + \rho g(h + \overline{\eta})$$

Therefore, $\overline{P_{-h}} \frac{\partial h}{\partial x}$ can be written as,

$$\overline{P_{-h}} \frac{\partial h}{\partial x} = \overline{P_{dyn_{-h}}} \frac{\partial h}{\partial x} + \rho g(h + \overline{\eta}) \frac{\partial h}{\partial x}$$

or alternatively as

$$\frac{1}{\rho} \overline{P_{-h}} \frac{\partial h}{\partial x} = \frac{1}{\rho} \overline{P_{\text{dyn}_{-h}}} \frac{\partial h}{\partial x} + \frac{1}{2} \frac{\partial}{\partial x} \{g(h + \bar{\eta})^2\} - g(h + \bar{\eta}) \frac{\partial \bar{\eta}}{\partial x}.$$

Using the result the time averaged, depth integrated x momentum equation is given by

$$\begin{aligned} & \frac{\partial}{\partial t} \{ \bar{U}(h + \bar{\eta}) + \int_{-h}^{\bar{\eta}} \hat{u} dz \} + \frac{\partial}{\partial x} \{ \bar{U}^2(h + \bar{\eta}) + 2\bar{U} \int_{-h}^{\bar{\eta}} \hat{u} dz + \int_{-h}^{\bar{\eta}} \hat{u}^2 dz \\ & + \frac{1}{\rho} \int_{-h}^{\bar{\eta}} P dz - \frac{1}{2} g(h + \bar{\eta})^2 \} + \frac{\partial}{\partial y} \{ \bar{U}\bar{V}(h + \bar{\eta}) + \bar{U} \int_{-h}^{\bar{\eta}} \hat{v} dz + \bar{V} \int_{-h}^{\bar{\eta}} \hat{u} dz \\ & + \int_{-h}^{\bar{\eta}} \hat{u}\hat{v} dz \} = \frac{1}{\rho} \overline{P_{\text{dyn}_{-h}}} \frac{\partial h}{\partial x} - g(h + \bar{\eta}) \frac{\partial \bar{\eta}}{\partial x} + \frac{1}{\rho} \overline{\tau_{sx}} - \frac{1}{\rho} \overline{\tau_{bx}} \\ & - \frac{\partial}{\partial x} \int_{-h}^{\bar{\eta}} \overline{u'^2} dz - \frac{\partial}{\partial y} \int_{-h}^{\bar{\eta}} \overline{u'v'} dz \end{aligned} \quad (9)$$

The quantities called the radiation stresses, or the excess momentum fluxes due to the presence of waves are defined as follows,

$$S_{xx} \equiv \int_{-h}^{\bar{\eta}} (P + \rho \hat{u}^2) dz - \frac{1}{2} \rho g(h + \bar{\eta})^2 - \frac{1}{\rho(h + \bar{\eta})} \left\{ \int_{-h}^{\bar{\eta}} \rho \hat{u} dz \right\}^2$$

$$S_{xy} \equiv \overline{\int_{-h}^{\eta} \rho \hat{u} \hat{v} dz} - \frac{1}{\rho(h + \bar{\eta})} \overline{\int_{-h}^{\eta} \rho \hat{v} dz} \overline{\int_{-h}^{\eta} \rho \hat{u} dz}$$

$$S_{yy} \equiv \overline{\int_{-h}^{\eta} (P + \rho \hat{v}^2) dz} - \frac{1}{2} \rho g (h + \bar{\eta})^2 - \frac{1}{\rho(h + \bar{\eta})} \overline{\left\{ \int_{-h}^{\eta} \rho \hat{v} dz \right\}^2}$$

The following assumptions will also be used:

- (1) The product of the wave induced pressure at the bottom and the bottom slope will be assumed negligible,
- (2) The gradient of the pressure due to turbulent fluctuations,

$$- \frac{\partial}{\partial x} \overline{\int_{-h}^{\eta} u'^2 dz}, \text{ is neglected, and}$$

- (3) The lateral friction caused by momentum fluxes due to turbulent fluctuations is assumed to be independent of depth.

This lateral friction will be called τ_l and is defined as $\overline{\tau_l} \equiv \overline{-\rho u'v'}$.

Finally letting the total depth D be defined as $D \equiv (h + \bar{\eta})$, the x momentum equation in its final form can be written as,

$$\begin{aligned} \frac{\partial}{\partial t}(UD) + \frac{\partial}{\partial x}(U^2 D) + \frac{\partial}{\partial y}(UV D) &= -gD \frac{\partial \bar{\eta}}{\partial x} - \frac{D}{\rho} \frac{\partial \overline{\tau_l}}{\partial y} \\ &- \frac{1}{\rho} \frac{\partial S_{xy}}{\partial y} - \frac{1}{\rho} \frac{\partial S_{xx}}{\partial x} + \frac{1}{\rho} \overline{\tau_{sx}} - \frac{1}{\rho} \overline{\tau_{bx}} \end{aligned} \quad (10)$$

Following the same procedure the final form of the y momentum equation can be found to be,

$$\begin{aligned}
\frac{\partial}{\partial y} (VD) + \frac{\partial}{\partial x} (UVD) + \frac{\partial}{\partial y} (V^2 D) = -gD \frac{\partial \bar{\eta}}{\partial y} - \frac{D}{\rho} \frac{\partial \bar{\tau}_x}{\partial x} \\
- \frac{1}{\rho} \frac{\partial S_{xy}}{\partial y} - \frac{1}{\rho} \frac{\partial S_{yy}}{\partial y} + \frac{1}{\rho} \bar{\tau}_{sy} - \frac{1}{\rho} \bar{\tau}_{by} \quad .
\end{aligned}
\tag{11}$$

WAVE TRANSFORMATIONS INCLUDING WAVE-CURRENT INTERACTION

The equations which govern both wave refraction and shoaling as a result of wave-current interaction used in the model are those of Noda, et al. The original derivation can be found in the report presented by Noda, et al. The advantage of Noda's method is that it predicts the wave angles and wave heights at certain points rather than along a wave ray. This procedure lends itself well to use in the finite difference model because calculations are performed at points which lie in the center of rectangular grid elements which are part of a larger grid mesh.

Starting with a progressive linear gravity wave, the free surface can be written as,

$$\eta(x,y,t) = a(x,y,t) \cos\{\phi(x,y,t)\}$$

where a is the wave amplitude and ϕ is some phase function. A wave number vector can be defined as

$$\vec{k} \equiv \nabla \phi \tag{12}$$

and a wave scalar frequency can be defined as

$$\bar{\sigma} = - \frac{\partial \phi}{\partial t} \quad . \quad (13)$$

Using the mathematical property that the curl of a gradient is identically zero, it is shown that

$$\nabla \times \nabla \phi = 0$$

which implies that

$$\nabla \times \vec{k} = 0$$

This equality states that the wave number vector is irrotational; i.e., the wave in question cannot travel in circles. Assuming $\phi(x,y,t)$ is continuous

$$\frac{\partial}{\partial t} (\nabla \phi) = \nabla \frac{\partial \phi}{\partial t}$$

or substituting Equations (12) and (13) into the above expression, it is found that

$$\frac{\partial \vec{k}}{\partial t} + \nabla \bar{\sigma} = 0 \quad (14)$$

which is the classical conservation of waves equation.

For the case of a wave propagating on a current with velocity $\vec{u} = u\vec{i} + v\vec{j}$, it can be shown that the scalar frequency with respect to a stationary reference frame is

$$\bar{\sigma} = \sigma + \vec{k} \cdot \vec{u} \quad .$$

The wave frequency with respect to a moving reference frame is given by the dispersion relation,

$$\sigma^2 = gk \tanh kh \quad . \quad (15)$$

If it is also assumed that the wave number field changes slowly with time then from Equation (14)

$$\nabla(\sigma + \vec{k} \cdot \vec{u}) = 0$$

or

$$\sigma + \vec{k} \cdot \vec{u} = \text{constant} \quad . \quad (16)$$

This constant can be evaluated for the case where $\vec{u} = 0$ in which case $\sigma = \frac{2\pi}{T}$ where T is the wave period.

Equation (16) then becomes

$$\sigma + \vec{k} \cdot \vec{u} = \frac{2\pi}{T} \quad . \quad (17)$$

Using the coordinate system shown in Figure 1 and expanding Equations (12) and (17) into Cartesian coordinates and using the dispersion relation, the equations which govern wave refraction through wave-current interaction are given by

$$\cos \theta \left\{ \frac{\partial \theta}{\partial x} - \frac{1}{k} \frac{\partial k}{\partial y} \right\} + \sin \theta \left\{ \frac{\partial \theta}{\partial y} + \frac{1}{k} \frac{\partial k}{\partial x} \right\} = 0 \quad (18)$$

$$\{gk \tanh(kh)\}^{1/2} + uk \cos \theta + vk \sin \theta = \frac{2\pi}{T} \quad . \quad (19)$$

where θ, k, h, u and v are all functions that may vary in both the x and y directions.

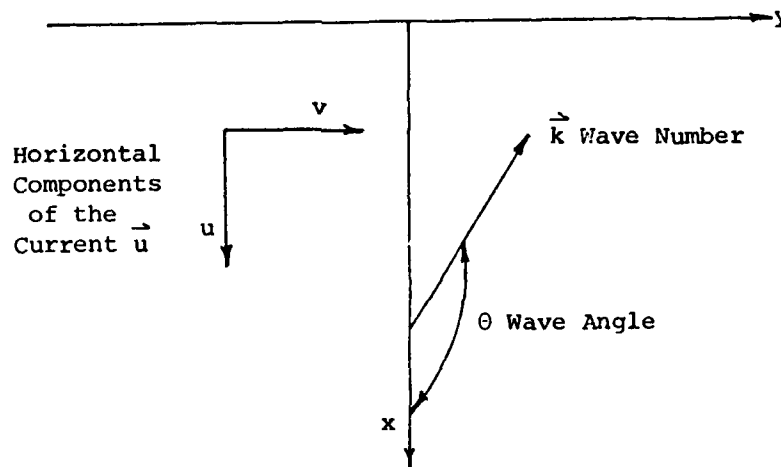


Figure 1 Planform Definition Sketch for the Wave Transformation Equations

The shoaling of waves is also affected by the interaction of waves and currents. The effect on the waves is determined by solving the energy equation. The form of the energy equation used in the model is the time averaged (over one wave period), depth integrated form for the case of a wave propagating on a current given by $\vec{u} = u\vec{i} + v\vec{j}$. Turbulent effects and dissipation are neglected in the derivation which can be found in Phillips (1966). His result is given by,

$$\begin{aligned} \frac{\partial E}{\partial t} + \frac{\partial}{\partial x} \{E(u + C_{gx})\} + \frac{\partial}{\partial y} \{E(v + C_{gy})\} + S_{xx} \frac{\partial u}{\partial x} \\ + S_{xy} \frac{\partial u}{\partial y} + S_{yy} \frac{\partial v}{\partial y} + S_{yx} \frac{\partial v}{\partial y} = 0 \end{aligned} \quad (20)$$

Dividing by E and expanding in Cartesian coordinates, Equation (20) can be written,

$$\begin{aligned} & \frac{1}{E} \frac{\partial E}{\partial t} + (u + C_g \cos \theta) \frac{1}{E} \frac{\partial E}{\partial x} + (v + C_g \sin \theta) \frac{1}{E} \frac{\partial E}{\partial y} \\ & + \frac{\partial}{\partial x} (u + C_g \cos \theta) + \frac{\partial}{\partial y} (v + C_g \sin \theta) \\ & + \frac{1}{E} \{ s_{xx} \frac{\partial u}{\partial x} + s_{xy} \frac{\partial u}{\partial y} + s_{yy} \frac{\partial v}{\partial y} + s_{xy} \frac{\partial v}{\partial x} \} = 0 . \end{aligned}$$

In the above equation, E is the total energy, both potential plus kinetic of a progressive linear water wave and is given by

$$E = \frac{1}{8} \rho g H^2$$

where H is the wave height.

Using this result, carrying out the differentiation, and letting a quantity Q be defined as

$$Q \equiv \frac{1}{E} \{ s_{xx} \frac{\partial u}{\partial x} + s_{xy} \frac{\partial u}{\partial y} + s_{xy} \frac{\partial v}{\partial x} + s_{yy} \frac{\partial v}{\partial y} \}$$

the energy equation becomes,

$$\begin{aligned} & \frac{2}{H} \frac{\partial H}{\partial t} + (u + C_g \cos \theta) \frac{2}{H} \frac{\partial H}{\partial x} + (v + C_g \sin \theta) \frac{2}{H} \frac{\partial H}{\partial y} + \frac{\partial u}{\partial x} + \frac{\partial v}{\partial y} \\ & - C_g \sin \theta \frac{\partial \theta}{\partial x} + \cos \theta \frac{\partial C_g}{\partial x} + C_g \cos \theta \frac{\partial \theta}{\partial y} + \sin \theta \frac{\partial C_g}{\partial y} + Q = 0 . \end{aligned} \quad (21)$$

For all applications of the model the wave height H is assumed constant in time so $\frac{\partial H}{\partial t} = 0$. From linear wave theory the group velocity C_g is given by

$$C_g = \frac{C}{2} \left\{ 1 + \frac{2kh}{\sinh(2kh)} \right\}$$

where

$$C = \left\{ \frac{g}{k} \tanh(kh) \right\}^{1/2}$$

is the wave speed or celerity, k is the wave number, and h is the water depth.

RADIATION STRESSES

In the derivation of the momentum equations the radiation stress terms S_{xx} , S_{xy} and S_{yy} were defined. Those forms can be simplified, and it has been shown, Longuet-Higgins and Stewart (1962), that to second order for a progressive, linear, small amplitude wave they can be approximated by,

$$S_{xx} = E \{ (2n-1/2) \cos^2 \theta + (n-1/2) \sin^2 \theta \}$$

$$S_{xy} = En \cos \theta \sin \theta$$

$$S_{yy} = E \{ (2n-1/2) \sin^2 \theta + (n-1/2) \cos^2 \theta \}$$

where E is the wave energy, θ is the wave angle, and n is the ratio of group velocity to wave celerity:

$$E \equiv \frac{1}{8} \rho g H^2$$

$$n \equiv \frac{C_g}{C} = \frac{1}{2} \left(1 + \frac{2kh}{\sinh 2kh} \right)$$

where

$$k = \text{wave number } (= \frac{2\pi}{L})$$

$$L = \text{wave length}$$

$$h = \text{water depth} \quad \text{and}$$

$$H = \text{wave height.}$$

WIND STRESS

The capability to handle a wind stress was retained from the work of Birkemeier and Dalrymple (1975). The wind stress is included as the surface stress in the horizontal momentum equations. No wind effects were included in applications of the present version of the model. A brief summary of the wind stress formulation is given below.

The form for the wind stress terms was assumed to be

$$\overline{\tau_{sx}} = \rho \kappa |w| w_x$$

$$\overline{\tau_{sy}} = \rho \kappa |w| w_y$$

where w is the magnitude of the wind speed and w_x and w_y are the x and y horizontal components of the wind speed. The density of water is ρ and the wind stress coefficient κ is based on the work of Van Dorn (1953) and assumed to be a function of the wind speed such that

$$\kappa = \kappa_1 \quad \text{for} \quad w \leq w_c$$

$$\kappa = \kappa_1 + \kappa_2 \left(1 - \frac{w_c}{w}\right)^2 \quad \text{for} \quad w \geq w_c$$

w_c is a critical wind speed taken as 14 knots and the coefficients κ_1 and κ_2 are taken to be 1.1×10^{-6} and 2.5×10^{-6} , respectively. A comparison of this coefficient, κ , with real data is given in the work of Pearce (1972).

BOTTOM STRESS

The bottom friction used in the model is of the quadratic form

$$\overline{\tau_b} = \frac{1}{8} \rho f \overline{u_t^+ |u_t^+|}$$

where "—" again denotes the time average over one wave period. The total velocity vector \vec{u}_t is comprised of both mean currents and wave orbital velocities. The quantities ρ and f are the water density and the Darcy-Weisbach friction factor, respectively. Referring to Figure 2, the mean current, \vec{u} , can be broken into its x and y components u and v .

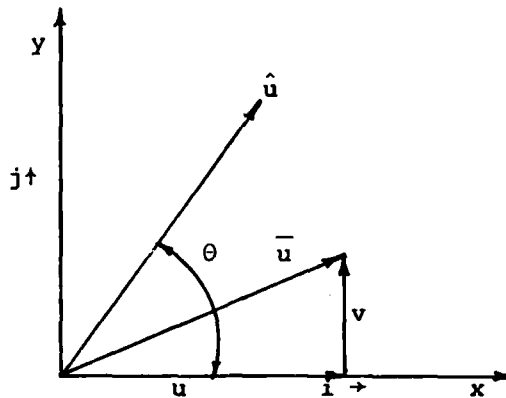


Figure 2 Definition Sketch for the Bottom Friction Formulation

The wave angle is given by theta and \vec{i} and \vec{j} are unit vectors in the x and y directions.

The total velocity vector \vec{u}_t can be expressed as

$$\vec{u}_t = (u + \hat{u} \cos \theta) \vec{i} + (v + \hat{u} \sin \theta) \vec{j}$$

whose magnitude is given by,

$$|\vec{u}_t| = \sqrt{u^2 + v^2 + \hat{u}^2 + 2u\hat{u}\cos \theta + 2v\hat{u}\sin \theta} \quad .$$

The wave orbital velocity \hat{u} can be expressed as

$$\hat{u} = \hat{u}_m \cos \sigma t \quad ,$$

where \hat{u}_m , the maximum wave orbital velocity, is

$$\hat{u}_m = \frac{\pi \eta}{T \sinh kh} .$$

The x and y components of the time averaged bottom friction then become,

$$\overline{\tau_{bx}} = \frac{\rho f}{16\pi} \int_0^{2\pi} (u + \hat{u}_m \cos \theta \cos \sigma t) \cdot |\vec{u}_t| d(\sigma t) \quad (22)$$

$$\overline{\tau_{by}} = \frac{\rho f}{16\pi} \int_0^{2\pi} (v + \hat{u}_m \sin \theta \cos \sigma t) \cdot |\vec{u}_t| d(\sigma t) \quad (23)$$

where $|\vec{u}_t|$ can now be written as,

$$|\vec{u}_t| = \sqrt{u^2 + v^2 + \hat{u}_m^2 \cos^2 \sigma t + 2u\hat{u}_m \cos \sigma t \cos \theta + 2v\hat{u}_m \cos \sigma t \sin \theta} .$$

Both of these stress components $\overline{\tau_{bx}}$ and $\overline{\tau_{by}}$ are of the form

$$\overline{\tau_b} = \frac{\rho f}{16\pi} \int_0^{2\pi} f(\sigma t) d(\sigma t) \quad (24)$$

or

$$\overline{\tau_b} = \frac{\rho f}{16\pi} S_n$$

where S_n is a sum of terms to approximate the integral in Equation (24) by Simpson's Rule:

$$S_n = \frac{\Delta(\sigma t)}{3} \{ f_0(\sigma t) + 4f_1(\sigma t) + 2f_2(\sigma t) + 4f_3(\sigma t) + \dots \\ + 2f_{n-2}(\sigma t) + 4f_{n-1}(\sigma t) + f_n(\sigma t) \} \quad (25)$$

where n is some positive even integer and

$$\Delta(\sigma t) = \frac{2\pi}{n} .$$

To find the x component of the shear stress the sum S_n can be found by taking the integrand in Equation (22) for the function $f(\sigma t)$. Similarly, for the y direction the function $f(\sigma t)$ is given by the integrand in Equation (23). The value of n was chosen to be 16. This choice was based on a comparison between the increased accuracy achieved with an n value greater than 16 and the increased computation time associated with a higher n value.

LATERAL MIXING

In a paper by Longuet-Higgins (1970), the author presented a formulation for the steady state velocity distribution as a result of waves breaking on a plane beach at some angle to the beach normal. This formulation was based on a balance between the bottom friction and the excess momentum flux in the longshore direction due to the presence of waves. The resulting longshore velocity distribution increased linearly from zero at the beach to its maximum at the breaker line. Outside the breaker line the velocity was everywhere zero.

However, physical observation and both laboratory and field data indicate that mean longshore flows are present beyond the

breaker zone. In a companion paper Longuet-Higgins presented a formulation which included lateral mixing as the means for the alteration of the linear velocity distribution into profiles found in nature as shown in Figure 3. These profiles have the discontinuity

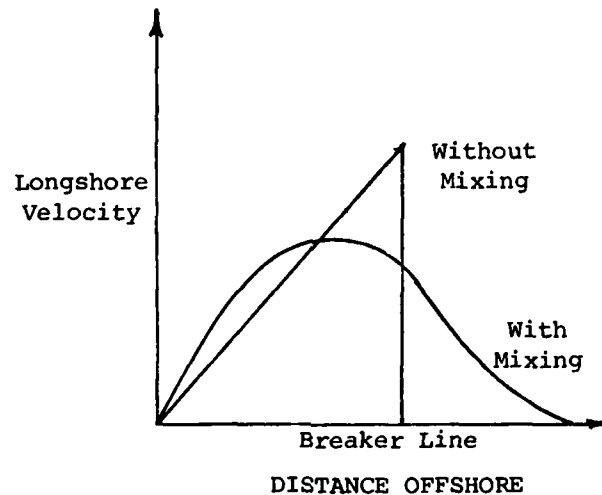


Figure 3 Longuet-Higgins' Analytical Solution for Oblique Wave Attack on a Plane Beach

at the breaker line removed and the peak velocity shifted shoreward. The velocities do tend to zero some distance outside of the breaker line.

There is a physical model to explain the mechanism of mixing and it is based on momentum exchange between fluid elements as they fluctuate. Consider a velocity distribution as shown in Figure 4. Allow the fluid element at x_1 with mean velocity v_1 to have a turbulent fluctuation u' in the direction parallel to the x axis.

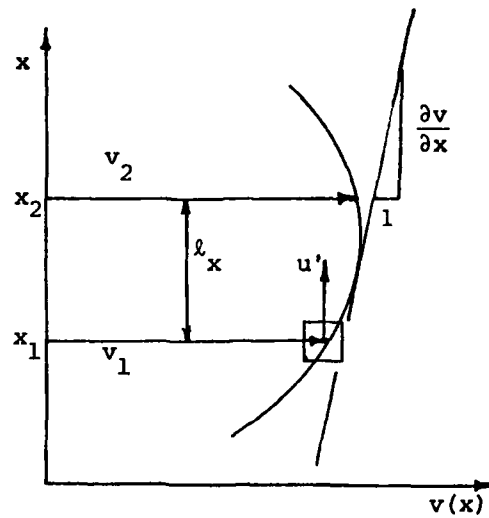


Figure 4 Definition Sketch for the Lateral Mixing Formulation

If this fluctuation u' caused the fluid element to move to its new position x_2 , then the element would be accelerated by the faster moving fluid with velocity v_2 , thereby increasing the momentum of the fluid element. The flux of momentum in translating fluid from x_1 to x_2 is $\rho u'$. Multiplying by $-v'$ which is the difference in velocities between the two fluid layers gives the momentum change per unit time in the direction of the mean flow or conversely, the shear stress exerted by the fluid layer at x_1 on the fluid layer at x_2 given by $\tau = -\rho u'v'$. The negative sign is a consequence of a positive turbulent velocity u' causing a negative shear stress because the layer at x_2 is impeded by the fluctuation of the fluid element from layer 1.

Using a Taylor series approximation to first order between the points x_1 and x_2 to find an expression for v' gives,

$$v' = v_2 - v_1 = (v_1 + \ell_x \frac{\partial v}{\partial x}) - v_1 = \ell_x \frac{\partial v}{\partial x} .$$

Therefore, the lateral shear stress between the fluid layers can be written as,

$$\tau = -\rho u' \ell_x \frac{\partial v}{\partial x} .$$

Since for an arbitrary coordinate system the velocity distribution could vary in two directions the shear could also include a term

$$\tau = -\rho v' \ell_y \frac{\partial u}{\partial y} .$$

For this reason the lateral shear stress τ_ℓ will be assumed to be,

$$\tau_\ell \propto -\rho (v' \ell_y \frac{\partial u}{\partial y} + u' \ell_x \frac{\partial v}{\partial x}) .$$

Two coefficients of lateral mixing, one for each direction x and y , are defined such that,

$$\epsilon_x \equiv u' \ell_x \quad \text{and} \quad \epsilon_y \equiv v' \ell_y .$$

The lateral shear stress is finally written as

$$\tau_\ell = -\rho (\epsilon_y \frac{\partial u}{\partial y} + \epsilon_x \frac{\partial v}{\partial x})$$

Longuet-Higgins argued that the mixing coefficient ϵ_x must tend to zero as the shoreline was approached since the turbulent eddies responsible for mixing cannot be of a scale greater than the distance to shore. He assumed that ϵ_x is proportional to the distance offshore, x , multiplied by some velocity scale which he chose to be \sqrt{gh} , the speed of a wave in shallow water where h is the local water depth. Therefore, ϵ_x can be written as

$$\epsilon_x = Nx \sqrt{gh}$$

where N is a dimensionless constant whose limits Longuet-Higgins gave as

$$0 \leq N \leq 0.016 \quad .$$

In this model the coefficient, ϵ_x , was allowed to vary linearly with x to some value around the breaker line. From this point seaward the coefficient remained at this constant value. The reason for this approximation is that physically there must be some limit on the scale of these eddies. This limit is at present not known. The coefficient, ϵ_y , was chosen to be constant. It is important to note that the purpose of the model is to present a stable numerical scheme which includes the effects of mixing. It is not an attempt to verify the choice of the mixing coefficients used.

CHAPTER III FINITE DIFFERENCE FORMULATION

At this point we have established a set of three governing equations, both mass and momentum, to be solved along with wave transformation equations and forcing terms from the momentum equations. This set of equations cannot be solved analytically so another method of solution must be found. In this chapter a means for solving the mass, momentum, and wave transformation equations numerically is presented. In the following chapter the boundary and initial conditions will be formulated along with the actual solution technique.

To solve the problem numerically a numerical scheme must be defined which leads to a systematic method of solution. This requires the following: (1) a breakdown of the area under study into a well defined grid system with a systematic way of defining variables of interest, and (2) the conversion of the governing equations into their finite differenced forms.

A rectangular grid mesh was established over the area of interest as shown in Figure 5 where x and y denote the offshore and longshore directions, respectively. The size of the grid blocks is

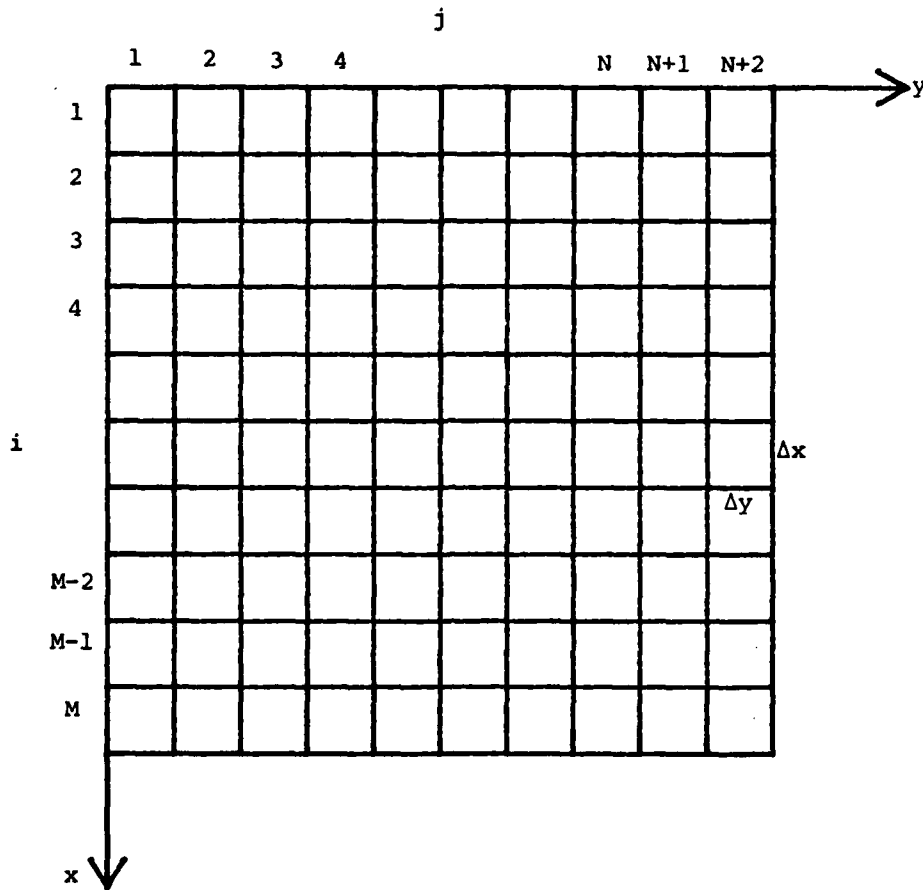


Figure 5 Grid Scheme Definitions

given by Δx in the x direction and Δy in the y direction. At each grid block, designated by the subscripts i and j as shown in Figure 6, certain variables must be defined. The velocities $u_{i,j}$ and $v_{i,j}$ are defined as being positive if they enter the i,j grid block in the positive x and y directions. Every other variable will be defined

at the grid center. The choice of this definition scheme lends itself well to the boundary conditions used in the model.

The methods used to transform the continuity and momentum equations into their differenced forms will be dealt with in detail. The derivation for the other equations will be mentioned only briefly. Again, the more detailed derivation can be found in Birkemeier and Dalrymple. Following the methods of Blumberg (1977) and Lilly (1965), certain operators are used throughout the derivation of the integrated mass and momentum equations. The first two operators are essentially central finite differences and are given by,

$$\delta_x \{F(x,y,t)\} \equiv \frac{1}{\Delta x} \left\{ F\left(x + \frac{\Delta x}{2}, y, t\right) - F\left(x - \frac{\Delta x}{2}, y, t\right) \right\}$$

$$\delta_x \{\overline{F(x,y,t)}\} \equiv \frac{1}{2\Delta x} \left\{ F(x + \Delta x, y, t) - F(x - \Delta x, y, t) \right\} .$$

In the first case the differencing takes place over one spacial grid (Δx) and in the second case, over two full grids ($2\Delta x$). Also defined are the following two operators which are merely averages in space, first in one direction, then in two.

These are given by,

$$\overline{F(x,y,t)}^x \equiv \frac{1}{2} \left\{ F\left(x + \frac{\Delta x}{2}, y, t\right) + F\left(x - \frac{\Delta x}{2}, y, t\right) \right\}$$

$$\overline{F(x,y,t)}^{xy} \equiv \overline{\overline{F(x,y,t)}^x}^y .$$

Note that in all four operators, $F(x,y,t)$ is some arbitrary function which varies in space and time. Similar operators also exist for time t and in the other horizontal dimension, y .

The governing continuity and momentum equations, Equations (6), (10) and (11), can be written in the following differenced forms,

CONTINUITY:

$$\delta_t(\overline{\eta^t}) + \delta_x(\overline{D^x u}) + \delta_y(\overline{D^y v}) = 0 \quad (26)$$

x MOMENTUM:

$$\begin{aligned} \delta_t(\overline{D^x u}) + \delta_x(\overline{D^x u} \overline{u^x}) + \delta_y(\overline{D^y v} \overline{u^y}) = \\ -g \overline{D^x} \delta_x(\eta) + \frac{1}{\rho} \overline{\tau_{sx}^x} - \frac{1}{\rho} \overline{\tau_{bx}^x} - \frac{1}{\rho} \delta_y(\overline{S_{xy}^{xy}}) \\ - \frac{1}{\rho} \delta_x(\overline{S_{xx}^{xx}}) + \overline{D^x} \delta_y \{ \epsilon_y \delta_y(u) \} + \overline{D^x} \delta_y \{ \epsilon_x^{xy} \delta_x(v) \} \end{aligned} \quad (27)$$

y MOMENTUM:

$$\begin{aligned} \delta_t(\overline{D^y v}) + \delta_x(\overline{D^x u} \overline{v^y}) + \delta_y(\overline{D^y v} \overline{v^y}) = \\ -g \overline{D^y} \delta_y(\eta) + \frac{1}{\rho} \overline{\tau_{sy}^y} - \frac{1}{\rho} \overline{\tau_{by}^y} - \frac{1}{\rho} \delta_y(\overline{S_{yy}^{yy}}) \\ - \frac{1}{\rho} \delta_x(\overline{S_{xy}^{xy}}) + \overline{D^y} \delta_x \{ \epsilon_y \delta_y(u) \} + \overline{D^y} \delta_x \{ \epsilon_x^{xy} \delta_x(v) \} \end{aligned} \quad (28)$$

It is important to note that when using the above differenced equations that the x,y coordinate is defined wherever the quantity to be solved for is defined. For example, since the x momentum equation is used to solve for the u velocity component, the x,y coordinate is located where $u_{i,j}$ is defined. In the continuity equation, the free surface displacement η is to be solved for so the x,y coordinate is defined to be at the center of the grid where $\eta_{i,j}$ is defined. This is important in converting from x,y notation into i,j notation.

In the i,j notation defined in Figure 6 these three governing equations become term by term,

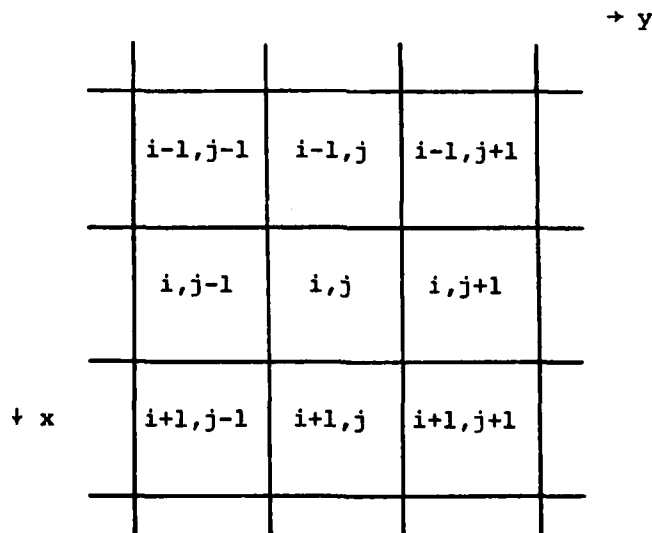


Figure 6 Differencing Coordinate (i,j) Sketch

CONTINUITY:

$$\delta_t(\overline{\eta^t}) = \frac{1}{2\Delta t} (\eta_{i,j}^{n+1} - \eta_{i,j}^{n-1})$$

$$\delta_x(\overline{D^x u}) = \frac{1}{2\Delta x} \{ (D_{i+1,j} + D_{i,j}) u_{i+1,j} - (D_{i,j} + D_{i-1,j}) u_{i,j} \} \quad (29)$$

$$\delta_y(\overline{D^y v}) = \frac{1}{2\Delta y} \{ (D_{i,j+1} + D_{i,j}) v_{i,j+1} - (D_{i,j} + D_{i,j-1}) v_{i,j} \}$$

x MOMENTUM:

$$\delta_t(\overline{D^x u}) = \frac{1}{4\Delta t} \{ (D_{i,j}^{n+1} + D_{i-1,j}^{n+1}) u_{i,j}^{n+1} - (D_{i,j}^{n-1} + D_{i-1,j}^{n-1}) u_{i,j}^{n-1} \}$$

$$\delta_x(\overline{D^x u u^x}) = \frac{1}{8\Delta x} \left[\{ (D_{i+1,j} + D_{i,j}) u_{i+1,j} + (D_{i,j} + D_{i-1,j}) u_{i,j} \} \cdot \right.$$

$$\left. \{ (u_{i+1,j} + u_{i,j}) \} - \{ (D_{i,j} + D_{i-1,j}) u_{i,j} + (D_{i-1,j} + D_{i-2,j}) u_{i-1,j} \} \cdot \{ (u_{i,j} + u_{i-1,j}) \} \right]$$

$$\delta_y(\overline{D^y v u^y}) = \frac{1}{8\Delta y} \left[\{ (D_{i,j+1} + D_{i,j}) v_{i,j+1} + (D_{i-1,j+1} + D_{i-1,j}) v_{i-1,j+1} \} \cdot \right.$$

$$\left. - \{ (u_{i,j} + u_{i,j+1}) \} - \{ (D_{i,j} + D_{i,j-1}) v_{i,j} + (D_{i-1,j} + D_{i-1,j-1}) v_{i-1,j} \} \cdot \{ (u_{i,j} + u_{i,j-1}) \} \right]$$

$$-g \overline{D^x} \delta_x(\eta) = -\frac{g}{2\Delta x} \{ (D_{i,j} + D_{i-1,j}) (\eta_{i,j} - \eta_{i-1,j}) \}$$

$$\frac{1}{\rho} \overline{\tau_{sx}^x} = \frac{1}{2\rho} (\tau_{sx\ i,j} + \tau_{sx\ i-1,j}) \quad (30)$$

$$-\frac{1}{\rho} \overline{\tau_{bx}}^x = -\frac{1}{2\rho} (\tau_{bx\ i,j} + \tau_{bx\ i-1,j})$$

$$-\frac{1}{\rho} \delta_y (\overline{s_{xy}}^{xy}) = -\frac{1}{4\Delta y \rho} (s_{xy\ i,j+1} - s_{xy\ i,j-1} + s_{xy\ i-1,j+1} - s_{xy\ i-1,j-1})$$

$$-\frac{1}{\rho} \delta_x (\overline{s_{xx}}) = -\frac{1}{\rho \Delta x} (s_{xx\ i,j} - s_{xx\ i-1,j})$$

$$\overline{D^x} \delta_y \{\epsilon_y \delta_y (u)\} = \frac{1}{2(\Delta y)^2} \{D_{i,j}^{n-1} + D_{i-1,j}^{n-1}\} \{\epsilon_y^{n-1} (u_{i,j+1}^{n-1} - u_{i,j}^{n-1}) -$$

$$\epsilon_y^{n-1} (u_{i,j}^{n-1} - u_{i,j-1}^{n-1})\}$$

$$\overline{D^x} \delta_y \{\epsilon_x^{xy} (v)\} = \frac{1}{8\Delta x \Delta y} \left[\{D_{i,j}^{n-1} + D_{i-1,j}^{n-1}\} \{(\epsilon_x^{n-1} u_{i,j+1}^{n-1} + \epsilon_x^{n-1} u_{i,j}^{n-1} + \epsilon_x^{n-1} u_{i-1,j}^{n-1} + \epsilon_x^{n-1} u_{i-1,j+1}^{n-1})\right.$$

$$\left. - (v_{i,j+1}^{n-1} - v_{i-1,j+1}^{n-1}) - (\epsilon_x^{n-1} u_{i,j}^{n-1} + \epsilon_x^{n-1} u_{i,j-1}^{n-1} + \epsilon_x^{n-1} u_{i-1,j-1}^{n-1} + \epsilon_x^{n-1} u_{i-1,j}^{n-1}) \cdot (v_{i,j}^{n-1} - v_{i-1,j}^{n-1})\} \right]$$

y MOMENTUM:

$$\delta_t (\overline{D^y v}) = \frac{1}{4\Delta t} \{(D_{i,j}^{n+1} + D_{i,j-1}^{n+1}) v_{i,j}^{n+1} - (D_{i,j}^{n-1} + D_{i,j-1}^{n-1}) v_{i,j}^{n-1}\}$$

$$\delta_x (\overline{D^x u v^y}) = \frac{1}{8\Delta x} \left[\{(D_{i+1,j} + D_{i,j}) u_{i+1,j} + (D_{i+1,j-1} + D_{i,j-1}) u_{i+1,j-1}\} \cdot \right.$$

$$\left. \{(v_{i+1,j} + v_{i,j})\} - \{(D_{i,j} + D_{i-1,j}) u_{i,j} + (D_{i,j-1} + D_{i-1,j-1}) u_{i,j-1}\} \cdot \{(v_{i,j} + v_{i-1,j})\} \right]$$

$$\delta_y (\overline{D^y v v^y}) = \frac{1}{8\Delta y} \left[\{(D_{i,j+1} + D_{i,j}) v_{i,j+1} + (D_{i,j} + D_{i,j-1}) v_{i,j}\} \cdot \right.$$

$$\{ (v_{i,j+1} + v_{i,j}) \} - \{ (D_{i,j} + D_{i,j-1}) v_{i,j} + (D_{i,j-1} + D_{i,j-2}) v_{i,j-1} \} \cdot \{ (v_{i,j} + v_{i,j-1}) \}]$$

$$-g \overline{D_y} \delta_y(\eta) = -\frac{g}{2\Delta y} (D_{i,j} + D_{i,j-1}) (\eta_{i,j} - \eta_{i,j-1})$$

(31)

$$\frac{1}{\rho} \overline{\tau_{sy}} = \frac{1}{2\rho} (\tau_{sy\ i,j} + \tau_{sy\ i,j-1})$$

$$-\frac{1}{\rho} \overline{\tau_{by}} = -\frac{1}{2\rho} (\tau_{bx\ i,j} + \tau_{by\ i,j-1})$$

$$-\frac{1}{\rho} \delta_y(S_{yy}) = -\frac{1}{\rho\Delta y} (S_{yy\ i,j} - S_{yy\ i,j-1})$$

$$-\frac{1}{\rho} \delta_x(\overline{S_{xy}}) = -\frac{1}{4\rho\Delta x} (S_{xy\ i+1,j-1} - S_{xy\ i-1,j-1} + S_{xy\ i+1,j} - S_{xy\ i-1,j})$$

$$\overline{D_x} \delta_x \{ \epsilon_y \delta_y(u) \} = \frac{1}{2\Delta x \Delta y} (D_{i,j}^{n-1} + D_{i,j-1}^{n-1}) \{ \epsilon_y^{n-1} (u_{i+1,j}^{n-1} - u_{i+1,j-1}^{n-1}) -$$

$$\epsilon_y^{n-1} (u_{i,j}^{n-1} - u_{i,j-1}^{n-1}) \}$$

$$\overline{D_x} \delta_x \{ \epsilon_x^{xy} \delta_x(v) \} = \frac{1}{8(\Delta x)^2} [(D_{i,j}^{n-1} + D_{i,j-1}^{n-1}) \{ (\epsilon_x^{n-1}{}_{i+1,j} + \epsilon_x^{n-1}{}_{i+1,j-1} + \epsilon_x^{n-1}{}_{i,j} + \epsilon_x^{n-1}{}_{i,j-1})$$

$$\cdot (v_{i+1,j}^{n-1} - v_{i,j}^{n-1}) - (\epsilon_x^{n-1}{}_{i,j} + \epsilon_x^{n-1}{}_{i,j-1} + \epsilon_x^{n-1}{}_{i-1,j} + \epsilon_x^{n-1}{}_{i-1,j-1}) (v_{i,j}^{n-1} - v_{i-1,j}^{n-1}) \}]$$

The superscripts $n, n+1, n-1$ denote the time level of a particular quantity. If the time level is not specified it is assumed to be equal to n . Also, the horizontal mixing terms are lagged in time for stability reasons, as mentioned in Holland and Lin (1975).

Looking back at the set of equations, Equations (18), (19) and (21), which govern the refraction and shoaling of waves through wave-current interaction, if Equation (19) is differentiated with respect to x to get $\frac{\partial k}{\partial x}$ and with respect to y to get $\frac{\partial k}{\partial y}$, these quantities can be substituted into Equation (18), which can then be written in the following form:

$$A \frac{\partial \theta}{\partial x} + B \frac{\partial \theta}{\partial y} = C \quad (32)$$

where A , B and C are functions of the quantities $\sin \theta$, $\cos \theta$, k , h , u and v . By taking a forward difference in x to approximate $\frac{\partial \theta}{\partial x}$ and a backwards difference in y to approximate $\frac{\partial \theta}{\partial y}$, Equation (32) becomes:

$$\theta_{i,j} = D + E \theta_{i,j-1} - F \theta_{i+1,j} \quad (33)$$

where D , E , and F are now functions of the quantities $\sin \theta_{i,j}$, $\cos \theta_{i,j}$, $k_{i,j}$, $h_{i,j}$, $u_{i,j}$, $v_{i,j}$. To evaluate $\sin \theta_{i,j}$ and $\cos \theta_{i,j}$ Noda used a first order Taylor series expansion to the four neighboring grids $i+1,j$, $i-1,j$, $i,j+1$ and $i,j-1$, summed the results and took an average value.

The theta field $\theta_{i,j}$ is solved for in the following way. Snell's Law is used to approximate the angles at the offshore row. Working shoreward Equation (33) is solved for in a row-by-row relaxation until the angles converge to their correct values with wave-current interaction included. After each updated value of theta, a new wave number must be solved for.

Equation (19) can be written as

$$E(k) \equiv \{gk \tanh(kh)\}^{1/2} + uk \cos \theta + vk \sin \theta - \frac{2\pi}{T} = 0 \quad (34)$$

To solve for the wave number, k , after each updated angle is found, the Newton-Raphson Method, or "method of tangents", is used. This method states that

$$k_{\text{new}} = k_{\text{old}} - \frac{E(k_{\text{old}})}{E'(k_{\text{old}})}$$

Differentiating Equation (34), k_{new} is iteratively solved for until $|k_{\text{new}} - k_{\text{old}}| \leq .001 |k_{\text{new}}|$.

The wave height field is calculated in much the same way as the wave angle field. Multiplying Equation (21) by $\frac{H}{2}$ and letting $\frac{\partial H}{\partial t} = 0$, the energy equation can now be written in the form

$$A \frac{\partial H}{\partial x} + B \frac{\partial H}{\partial y} = C H \quad (35)$$

where A , B and C are functions of u , v , $\cos \theta$, $\sin \theta$, C_g , Δx , Δy and the radiation stresses. Taking a forward difference in x to approximate $\frac{\partial H}{\partial x}$ and a backward difference in y to approximate $\frac{\partial H}{\partial y}$ and solving for $H_{i,j}$, it can be shown that

$$H_{i,j} = D H_{i,j-1} - E H_{i+1,j}$$

where D and E are functions of the same quantities as A, B and C.

Again the offshore row of wave heights are obtained from shoaling and refraction due to Snell's Law and the wave height field is determined by relaxing row by row in the shoreward direction.

On each row a solution for the wave height is reached when

$|H_{\text{new}} - H_{\text{old}}| \leq .01 H_{\text{new}}$. After each updated value of $H_{i,j}$, a breaking wave height is also calculated from the breaking criteria given by the Miche formula

$$\left(\frac{H}{L}\right)_b = .12 \tanh(kh)_b .$$

If the calculated $H_{i,j}$ is larger than the allowable breaking height, the height $H_{i,j}$ was set equal to the breaking height.

CHAPTER IV METHOD OF SOLUTION

In the previous chapter the three governing equations, conservation of both mass and horizontal momentum, were derived in their finite difference forms. The numerical procedure, used by Birkemeier and Dalrymple and Noda, et al., to calculate the wave characteristics used in the "forcing terms" in the momentum equations was also presented. In this chapter the initial and boundary conditions will be stated completing the problem formulation, whereupon a method of solution will be given.

In every application of the present model the initial conditions were assumed to be the state of rest. The velocity field, both u and v components as well as the mean free surface displacement, η , were initially set equal to zero. An initial depth field is inputted into the model and the wave characteristics, both angles and heights, were calculated initially using Snell's Law. The wave height was built up from zero to its full deep water value over a certain number of iterations using the hyperbolic tangent function in order to prevent "shock loading" the model. The form for this build-up is,

$$H = H_0 \tanh \left(\frac{2t}{T} \right)$$

where

H_0 = deep water wave height

t = time the model has progressed

T = time allowed for wave build-up.

Certain boundary conditions were also invoked. Referring to the grid system shown in Figure 5, no offshore flow was allowed into row m . This is represented by

$$u_{m,j} = 0$$

which essentially simulates a wall at the offshore end of the grid mesh. The reason behind this choice of boundary condition is this: at, or near, steady state, if row m is far enough offshore so that the effects of rip currents and longshore currents are negligible, the assumption of zero onshore-offshore velocity is valid. A more correct boundary condition would be to let the mean free surface be zero in deep water which would entail the addition of grid blocks offshore, thereby increasing computational time and expense. At the inshore end of the grid mesh no velocities were allowed to enter the first dry grid row. Again, this implies the existence of a wall at the beach boundary.

In the longshore direction periodic boundary conditions were imposed. Again referring to Figure 5, for any quantity, Q , periodicity

requires that,

$$Q(i,1) = Q(i,N)$$

$$Q(i,2) = Q(i,N+1)$$

$$Q(i,3) = Q(i,N+2)$$

and so forth. Periodic boundary conditions were used because circulation patterns along coastlines often tend to have a periodicity associated with them. Also if it is desired to model an arbitrary stretch of beach that has no periodicity, we can choose boundaries far enough away from this area of interest, such that periodic boundary conditions in the longshore direction become applicable.

The differenced mass and momentum equations from the preceding chapter were derived using a central difference in time for the time dependent terms. These three equations can also be written in the following abbreviated form,

$$\eta_{i,j}^{n+1} = \eta_{i,j}^{n-1} + 2\Delta t F_1 \quad (36)$$

$$u_{i,j}^{n+1} = A u_{i,j}^{n-1} + 2\Delta t F_2 \quad (37)$$

$$v_{i,j}^{n+1} = B v_{i,j}^{n-1} + 2\Delta t F_3 \quad (38)$$

where A and B are functions of the depth alone and F_1 , F_2 , and F_3 are functions of all the variables in the problem. Also remember that F_1 , F_2 , and F_3 contain quantities evaluated at time level, n, and n-1.

These three equations could have also been derived using a forward difference in time in which case,

$$\eta_{i,j}^{n+1} = \eta_{i,j}^n + \Delta t F_1 \quad (39)$$

$$u_{i,j}^{n+1} = C u_{i,j}^n + \Delta t F_4 \quad (40)$$

$$v_{i,j}^{n+1} = D v_{i,j}^n + \Delta t F_5 \quad (41)$$

This set of equations will be used to start the computation scheme as will be seen in the following discussion.

The problem has now been formulated with a set of three differenced, governing equations (Equations (36), (37), and (38)), initial conditions and boundary conditions. The next step is to develop a computational scheme to solve the problem. Given the initial conditions, the wave characteristics and the values of η , u , and v at time zero ($n=0$), the functions C , D , F_1 , F_4 , and F_5 , in the set of Equations (39) through (41), become known. Using a time step of $1/2\Delta t$ instead of Δt , to increase the accuracy of the first calculations, the new values of η , u , and v at time $n+1$ can be calculated. Knowing these new values the wave-current interaction equations can be solved to find wave heights, angles, and wave numbers at time $\Delta t/2$.

The next calculation is done using a computational scheme called the "leapfrog" technique, which uses the set of Equations (36-38). To employ the leapfrog scheme variables must be defined for the two previous time steps, which has been established using the initial conditions and the results from the first forward difference calculation. Referring to Figure 7, the variables are known at time levels $n-1$ and n . The functions F_1 , F_2 , F_3 , A and B are thus known and u , v , and η at time level $n+1$ can be calculated using the same time step of $1/2\Delta t$. The wave-current equations are again solved at time $n+1$ making all of the variables defined at 0 and Δt .

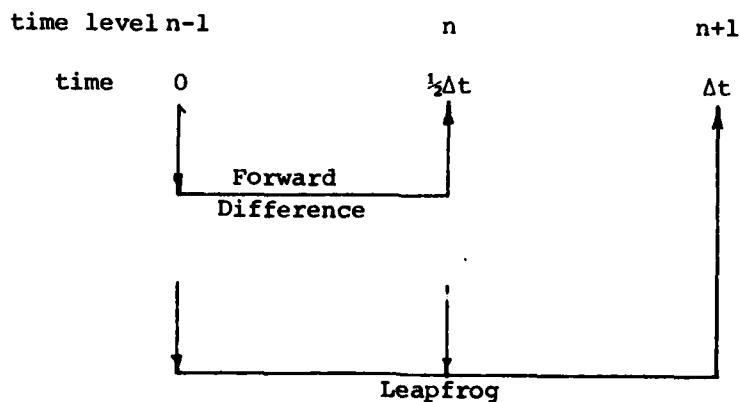


Figure 7 Initial Forward Difference and the First Leapfrog Solution Steps

The leapfrog scheme is now employed with a time step of Δt , illustrated in Figure 8. The quantities at time level $n+1$ are calculated knowing the quantities at time levels $n-1$ and n . This procedure continues throughout the remaining steps of computation except for a slight modification. Using strictly the leapfrog scheme for this particular set of equations resulted in a stability problem which will be discussed in the following chapter.

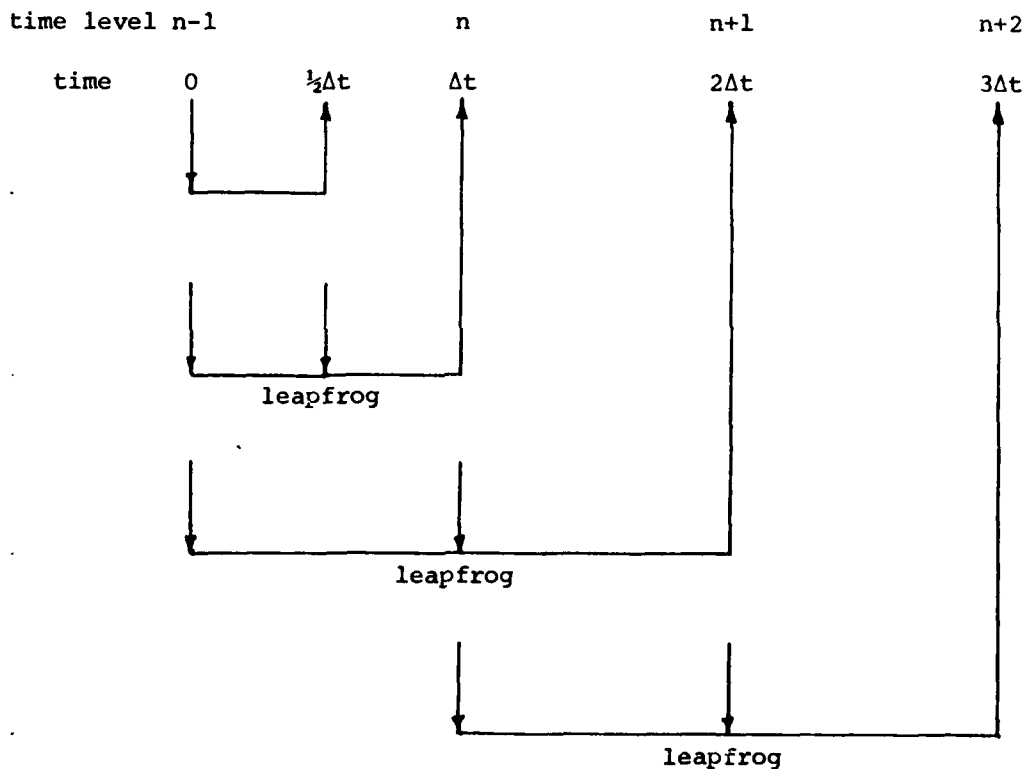


Figure 8 General Leapfrog Solution Scheme

CHAPTER V STABILITY ANALYSIS

The exact stability criteria for the full sets of equations used in the model cannot be determined analytically. In the applications of this model, stability can be expressed in the following manner. The speed of propagation of some disturbance in the model must be less than or equal to the speed it takes the disturbance to cross a computational grid block in a computational time step. If this criterion is not met, the model will not be able to "see" the disturbance.

The disturbance speed is in general the speed of a shallow water gravity wave plus some time independent mean current. Therefore, in general, the stability criteria can be expressed as,

$$\Delta t \leq \frac{\sqrt{(\Delta x)^2 + (\Delta y)^2}}{|u| + \sqrt{gh}}$$

The maximum magnitude of the wave speed exceeds the minimum current speed in general so the stability criterion used in applications of this model is,

$$\Delta t \leq \frac{\sqrt{(\Delta x)^2 + (\Delta y)^2}}{\sqrt{gh_{\max}}}$$

which is a type of two-dimensional Courant number. In all cases, the time step actually used is much less than that given by the above criteria. The determination of a better stability criteria and the probable limits on the time step were not investigated in much detail.

As mentioned in the preceding chapter an instability resulted from using the leapfrog technique to integrate the equations in time. As the model approached a steady state, the solution diverged into two disjoint solutions; one associated with the even time steps and the other the odd steps. These solutions oscillated with growing amplitudes about the steady state solution. In Roache (1972), the author referred to this as time splitting.

To alleviate the problem, a leapfrog-backward correction scheme, Kurihara (1965), was initiated every tenth time step. The scheme is shown below as,

$$h^* = h^{n-1} + 2\Delta t G^n \quad (42)$$

$$h^{n+1} = h^n + \Delta t G^* \quad (43)$$

where h may be u , v , or η . Equation (42) is simply the leapfrog calculation done by the Equations (36-38) where $*$ denotes the new or

"interim" time level. Using the new values u , v , η at time $*$, the functions G^* like the functions F_1 , F_2 , and F_3 from Equations (36-38) are calculated and used in Equation (43), which is merely a backwards difference in time to the level n .

This scheme was chosen because it damps the computational mode of the solution while leaving the physical mode relatively unaffected. For a more in-depth discussion the reader is referred to the work by Kurihara. With this correction scheme included, which essentially "ties" the solutions together, every tenth iteration, the model proceeded to reach a steady state without any further time-splitting instability.

CHAPTER VI RESULTS

PLANE BEACH APPLICATIONS

The model was first applied to the case of a single progressive wave train approaching a planar beach at some angle to the beach normal. Periodic boundary conditions were imposed in the longshore direction making the beach infinitely long. The purpose of this application was to compare the model to the earlier efforts of Birkemeier and Dalrymple and to the analytical work of Longuet-Higgins (1970) on longshore currents generated by obliquely incident waves.

For the series of plane beach runs, the same input data was used. The deep water wave characteristics were: (1) wave period of 8.0 seconds, (2) wave angle of 30.0 degrees from the beach normal, and (3) a wave height of 2.0 meters built up over 200 ($\Delta t = 0.5$ second) iterations. The time step of 0.5 seconds is well below the "allowable" value of about 1.8 seconds computed from the stability criteria presented in the previous chapter. The region of interest was broken into a 6 x 30 grid mesh with a grid

spacing of 10.0 meters in the x direction and 15.0 meters in the y direction. The beach slope was chosen to be 0.025 which resulted in water depths of 0.0 to 7.00 meters. In all runs the bottom friction factor, f , was chosen to be 0.08. When applicable, the mixing coefficients N and ϵ_y were chosen to be 0.01 and 0.5 meters/sec², respectively.

In each case the model was run for 1200 iterations which is nearly steady state. This is demonstrated in plots of mean free surface displacement, or velocity, versus time at selected grid points which, for the case using the present model without horizontal mixing, are shown in Figures 9 through 12. Note the dominant period of oscillation of about 112 seconds. This corresponds well to the seiche period (of 113 seconds) for the first mode of oscillation for a triangular basin given by the expression (Wilson, 1966),

$$T = \frac{3.28 L}{\sqrt{gh_{\max}}}$$

where, T = period of oscillation in the basin

L = length of the basin

h_{\max} = maximum depth in the basin.

The area of interest for the plane beach applications is essentially an infinitely long triangular basin as a result of the flow conditions imposed at the inshore and offshore boundaries.

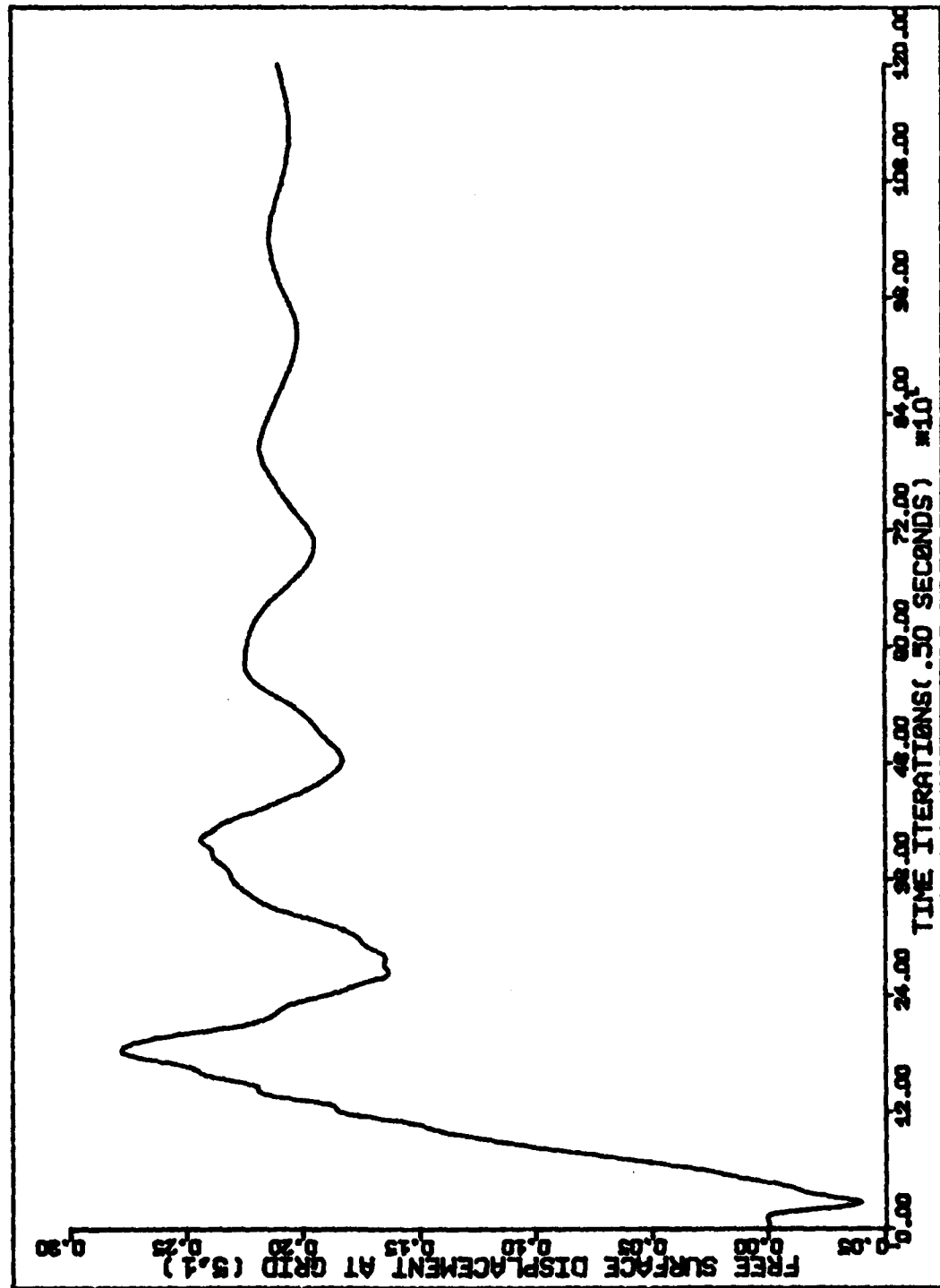


Figure 9 Plot of Inshore Mean Free Surface Displacement Versus Time for the Present Non-Linear Model Application to a Plane Beach

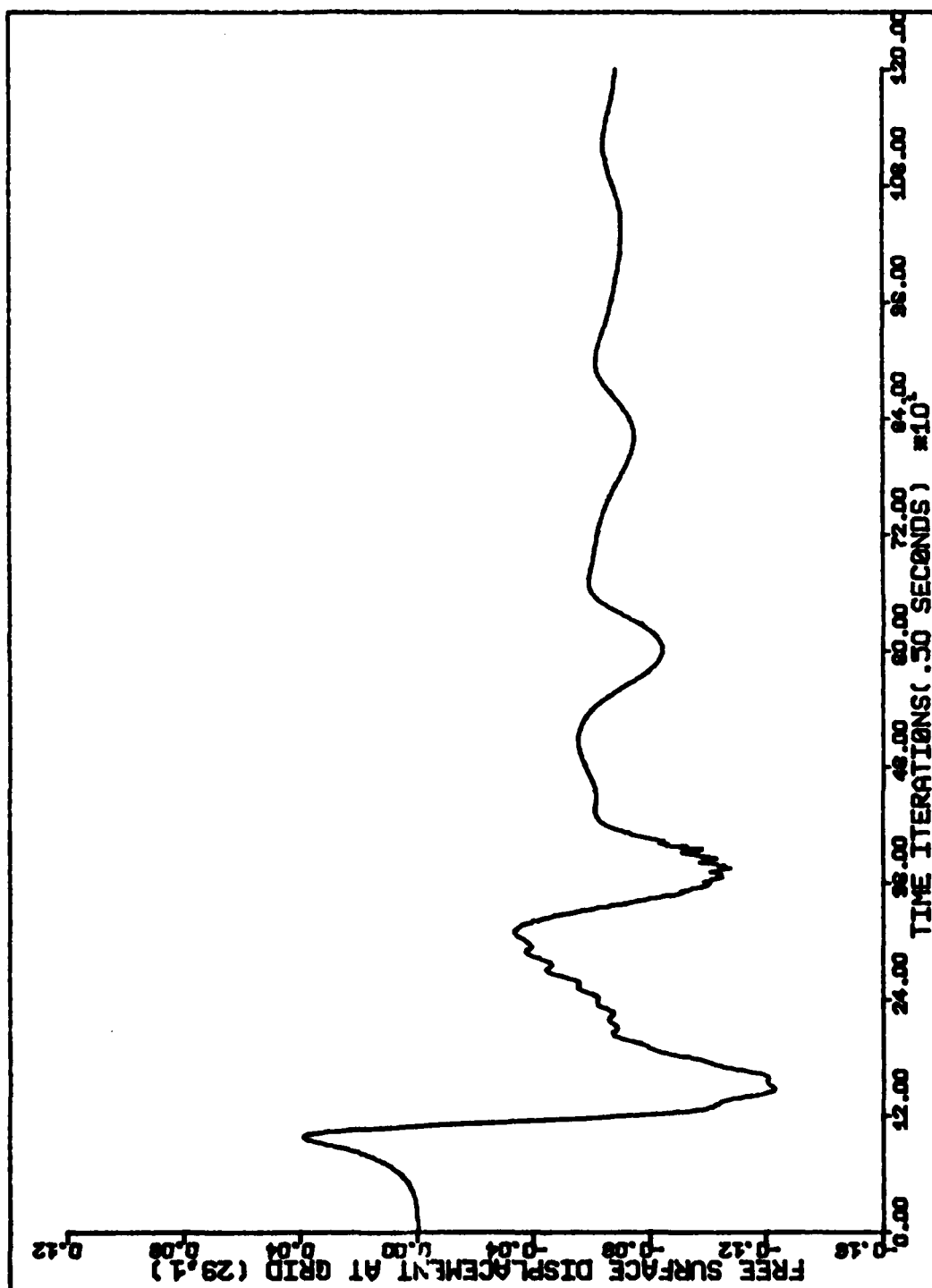


Figure 10 Plot of Offshore Mean Free Surface Displacement Versus Time
for the Present Non-Linear Model Application to a Plane Beach

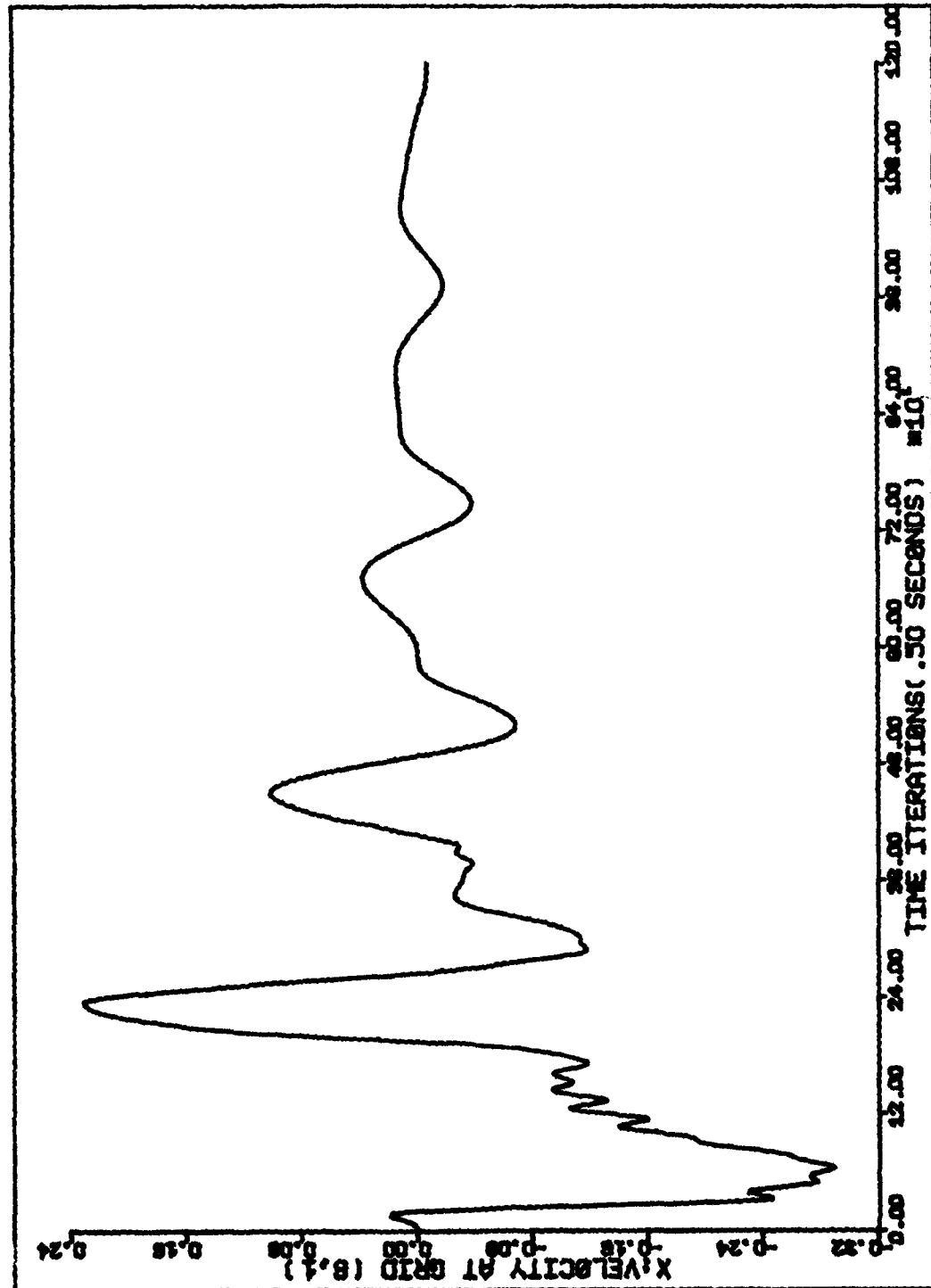


Figure 11 Plot of Inshore x-Velocity Component Versus Time for the Present Non-Linear Model Application to a Plane Beach

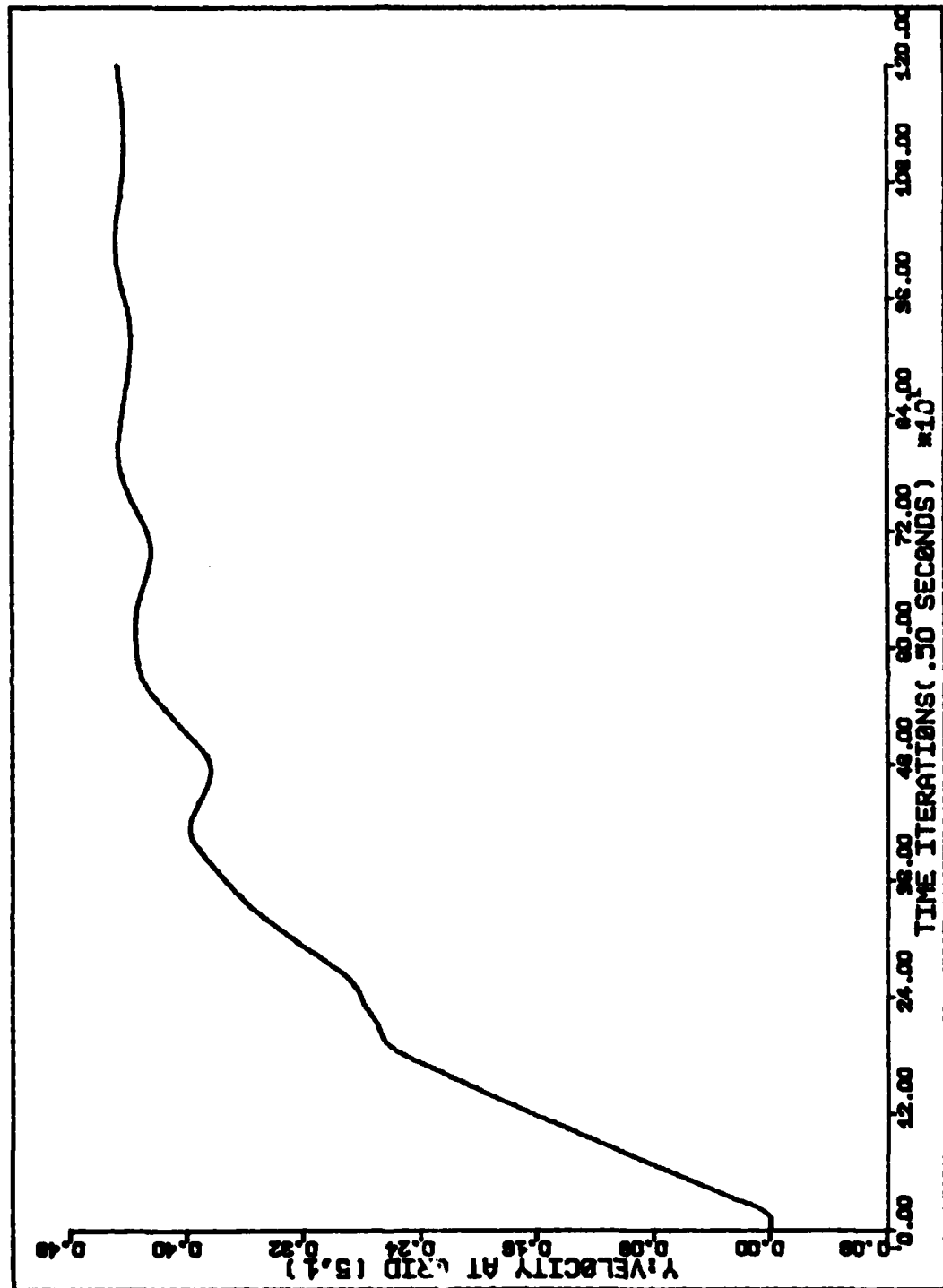


Figure 12 Plot of Inshore y-Velocity Component Versus Time for the Present Non-Linear Model Application to a Plane Beach

In the first run the data was inputted into the linear model of Birkemeier and Dalrymple. The resulting longshore current profile is shown in Figure 13. Note the monotonic increase in the magnitude of the velocity from zero at the dry beach to a maximum of about 1.15 meters per second, 110 meters offshore, which is approximately the location of the breaker line. From the maximum, the velocity decreases rapidly to zero and remains essentially zero outside the breaker line, indicating no offshore mixing effects.

Note the similarity between the form of this current profile and the form given by Longuet-Higgins (1970) analytical solution for the case of a wave approaching a planar beach at some oblique angle, neglecting the effects of mixing, as shown in Figure 3. The major difference between the two profiles is that the linear model result shows less of a discontinuity at the breaker line. This is caused by the use of a discrete, onshore-offshore grid size in the numerical model which obscures the breaker line. As this grid dimension is reduced the location of the breaker line becomes better defined thus reducing the effect of "breaker line smoothing" on the velocity distribution. Also associated with this grid size reduction is an increase in the magnitude of the peak velocity to something on the order of that predicted by Longuet-Higgins, which for the input data, is about 1.5 meters per second.

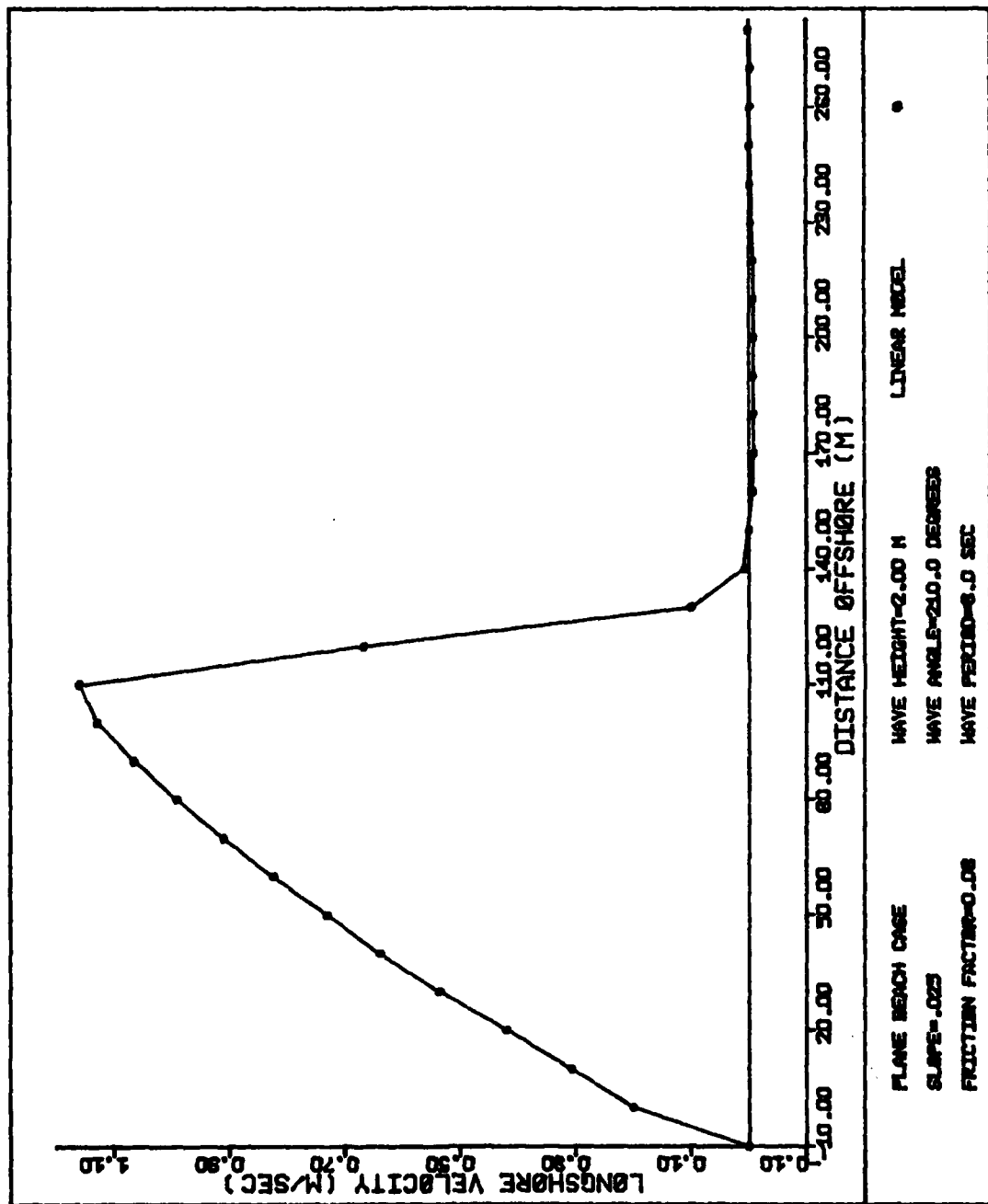


Figure 13 Longshore Current Profile for Plane Beach Case from Linear Model of Birkemeier and Dalrymple

A lesser point to note is that in all the plane beach applications, there is a slight discontinuity in the velocity profile at the inshore region. This is due to the fact that initially a small amount of water was placed in each block of the first "dry" grid row. As time proceeded, this block was then allowed to fill, in essence, simulating the effects of flooding. Had a procedure been implemented that would have allowed for the flooding of more than one grid row, this discontinuity would have disappeared.

Figure 14 shows the longshore current profile resulting from the present non-linear version of the model excluding the effects of horizontal mixing. The form is similar to the linear result except for the decrease in peak velocity and the extension of the profile a small distance outside the breaker zone. The existence of velocities outside the breaker zone is due to the fact that the advective acceleration terms in the differenced y momentum equation caused velocities outside the breaker zone to be calculated using velocities inside the breaker zone. The deviation between peak velocities predicted by the two models is attributed to the use of the quadratic, "exact" bottom friction formulation used in the non-linear model. Liu and Dalrymple (1978) showed that the use of this bottom friction term caused the peak velocities of Longuet-Higgins linear approximation to be decreased by about 20% for a breaking wave angle of around 10 degrees. In the plane beach applications of the linear and non-linear models the breaker angle is about 12 degrees and the discrepancy

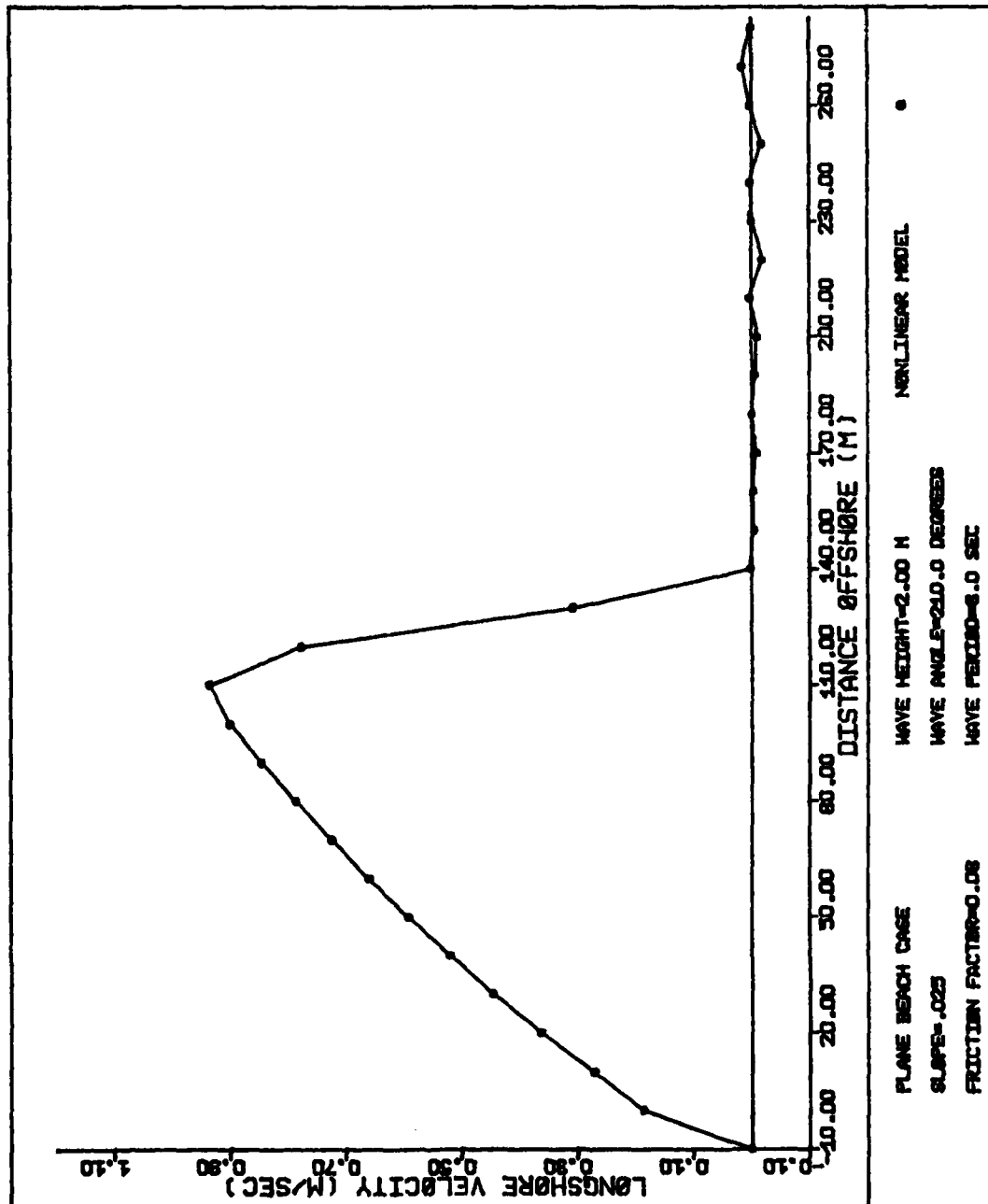


Figure 14 Longshore Current Profile for Plane Beach Case from Present Model Excluding Mixing

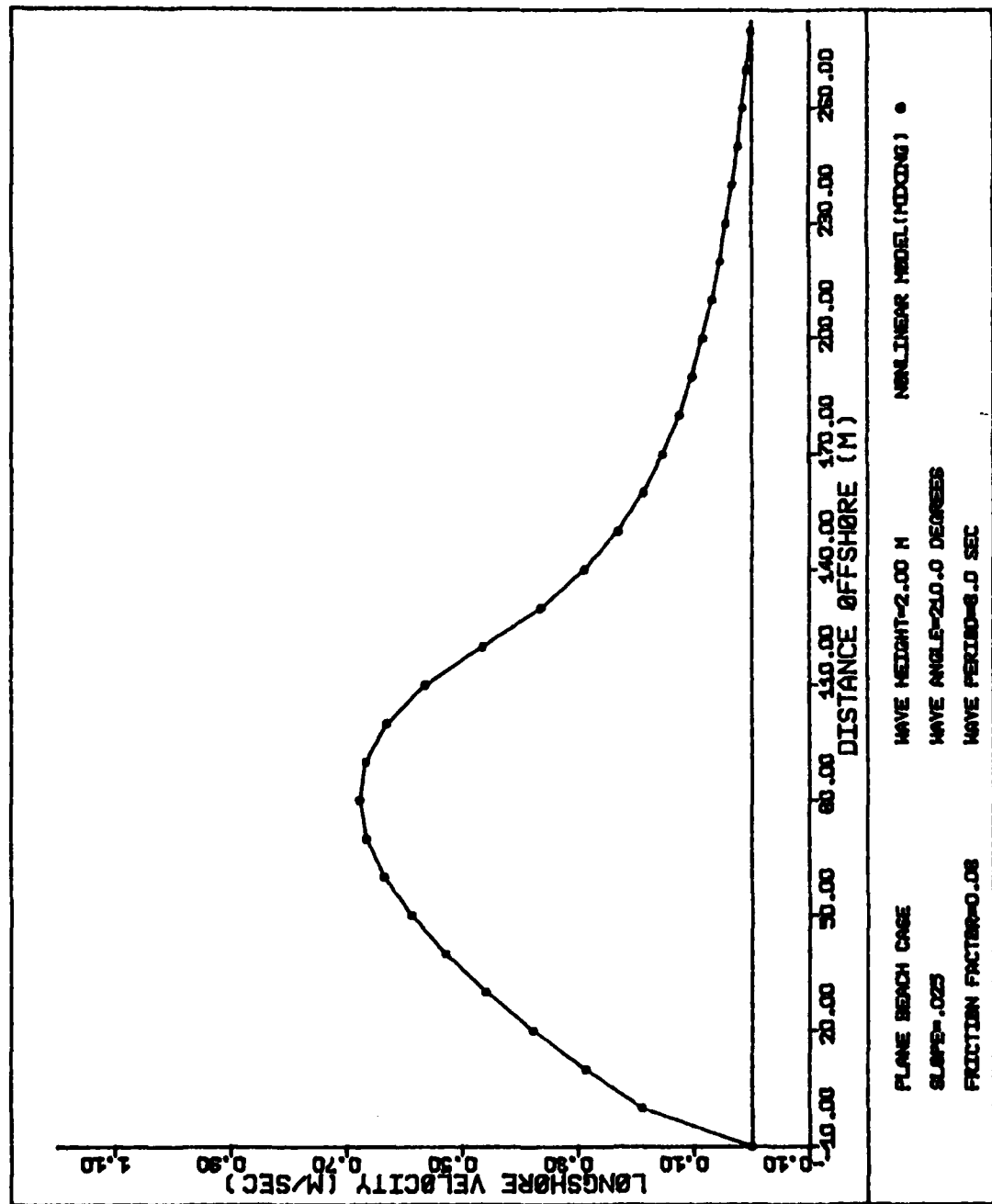


Figure 15 Longshore Current Profile for Plane Beach Case from Present Model Including Mixing

in peak velocities between the two models is about that same 20%.

The final run using the plane beach data was made with the non-linear model including lateral mixing. The steady state long-shore velocity profile is shown in Figure 15. This profile exhibits the following differences from that predicted by the model neglecting mixing:

- (1) in the inner one half of the surf zone the velocities are increased slightly,
- (2) the peak velocity is shifted to a new location shoreward of the breaker line, and
- (3) the velocity distribution extends well beyond the breaker line eventually decreasing towards zero.

The form of this profile is similar to the analytic result of Longuet-Higgins including the effects of mixing shown in Figure 3.

BARRED PROFILE APPLICATION

Since, in nature, beach topography is often comprised of fragmented longshore bars, the present version of the model was run on a bottom configuration that included an infinitely long longshore bar. A comparison of the barred profile with a planar beach (with a slope of 0.025) is shown in Figure 16. The remaining input into the model was identical to that used in the series of plane beach runs. The model was run both with and without the effects of mixing included.

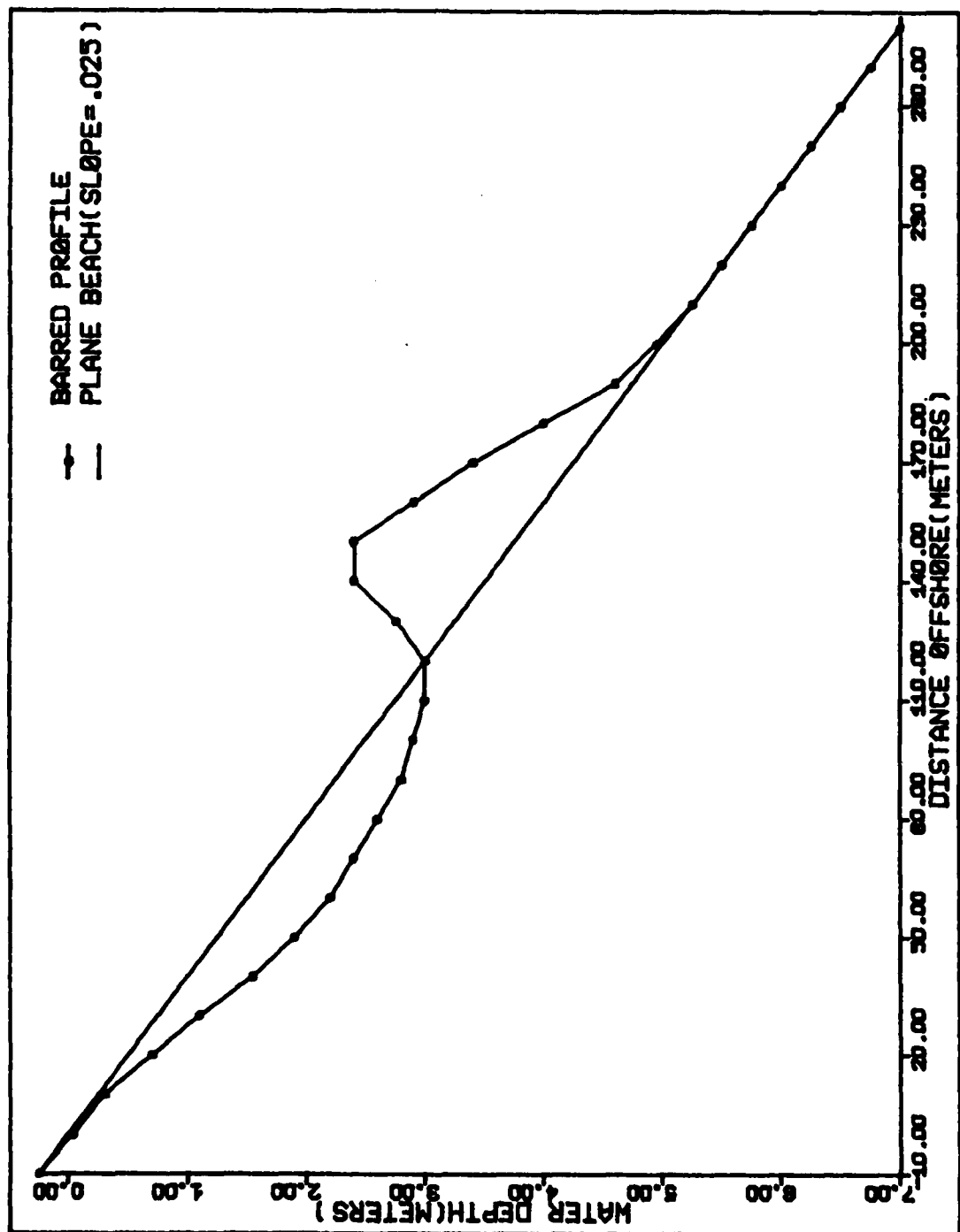


Figure 16 Comparison of Barred Profile and Plane Beach

The results for the case without mixing are shown in Figure 17. Notice the two distinct regions where a longshore current distribution exists. The velocity "spike" offshore is due to waves breaking on the bar. As the wave height decreases, as a result of breaking, an onshore-offshore gradient of y momentum flux is created which drives a longshore current. In the trough, however, the wave height starts to reform (no more breaking) resulting in the absence of a longshore current in this region. In reality, a longshore current does exist in the trough, Allender, et al. (1978), due to the mechanisms of turbulent dissipation during breaking within a bore, lateral mixing which has been included in the model, and a set-up of water within the trough, Dalrymple (1978).

Figure 18 shows the resulting longshore current profile for the model run including horizontal mixing. The effects of mixing are very much evident as the amplitude of the longshore velocity "spike" is reduced, the discontinuities in the velocity profile disappear, and a longshore current now exists in the bar trough. Had the turbulent energy dissipation mechanism been included in the model, the results would probably have approached those found in nature.

PERIODIC BOTTOM TOPOGRAPHY APPLICATION

The model was next applied to the periodic bottom topography developed by Noda, et al., which is essentially a channel at some

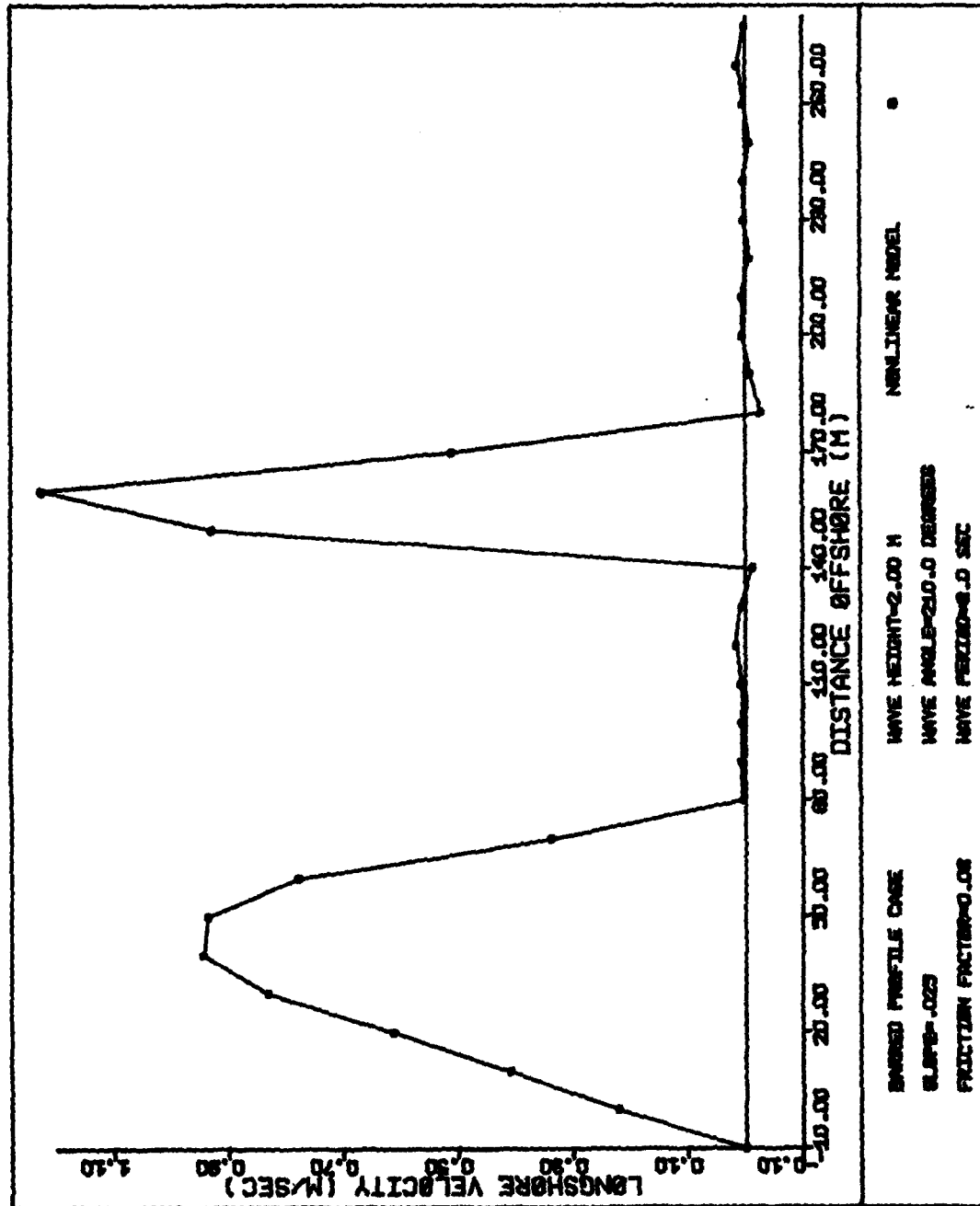


Figure 17 Longshore Current Profile for the Present Model Excluding Mixing Run on the Barred Profile

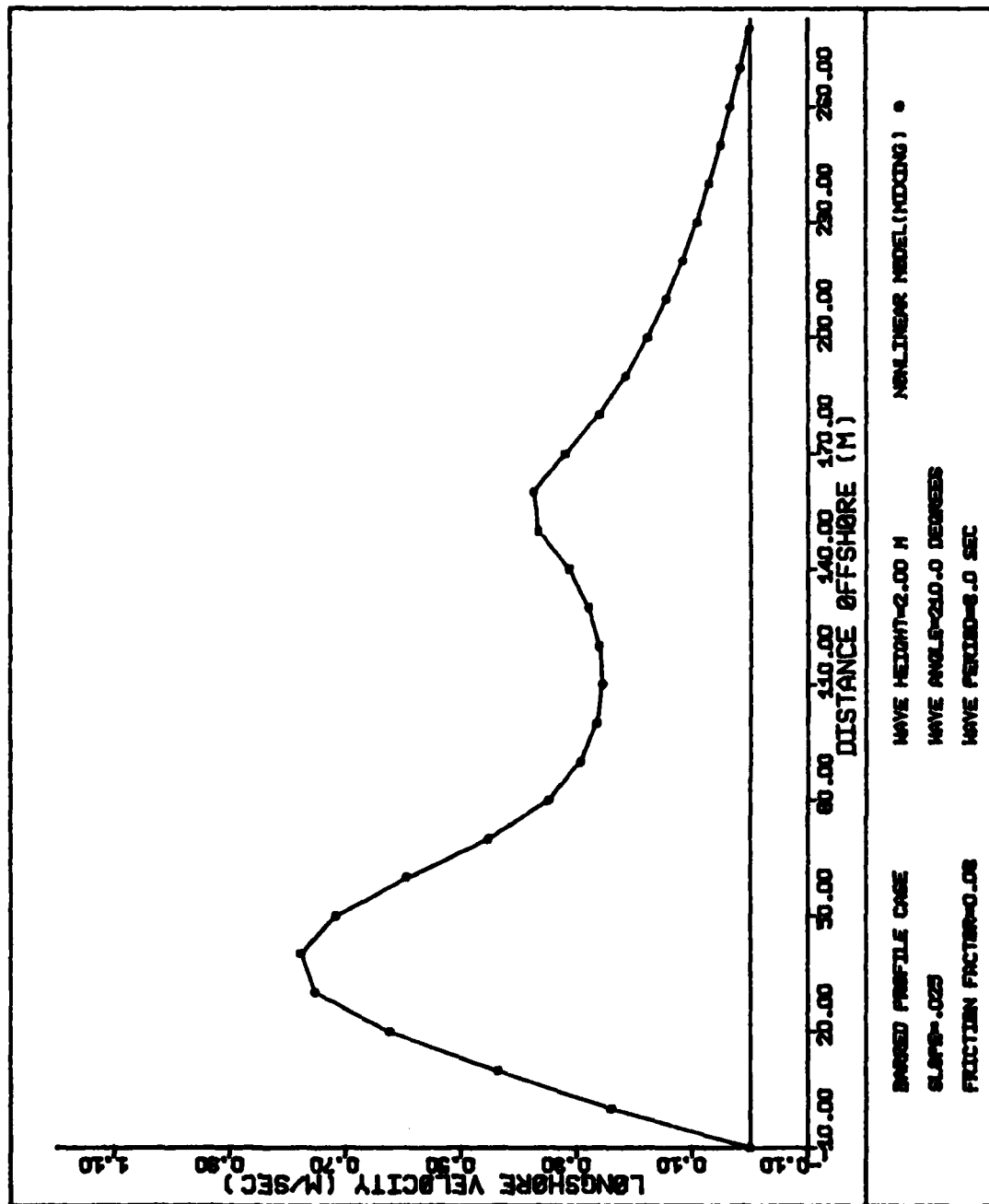


Figure 18 Longshore Current Profile for the Present Model Including Mixing Run on the Barred Profile

angle to the beach normal. The formulation for this bottom configuration is given in Appendix A. The present version of the model, including the effects of mixing, was compared to the linear model of Birkemeier and Dalrymple. The following wave characteristics were used in both instances:

- (1) deep water wave height of 1.0 meters,
- (2) wave period of 4.0 seconds, and
- (3) a deep water wave angle of 30.0 degrees to the beach normal.

The bottom friction factor, f , was chosen to be 0.08, and the mixing coefficients, N and ϵ_y , were chosen to be 0.005 and 0.5 m/sec^2 , respectively. In both runs the wave height was built up to its deep water value over 100 seconds.

Both models were run until they reached approximately a steady state, about 500 seconds. The wave-current interaction process was halted in the linear model after 150 seconds because the offshore velocity components grew too large for the refraction routines to handle. In the non-linear model, however, the wave-current interaction process was included for the duration of the run time. The circulation patterns after 500 seconds are shown in Figures 19 and 20.

Note the strength of the rip and its offshore extent in the linear model compared to non-linear model. The peak velocity in

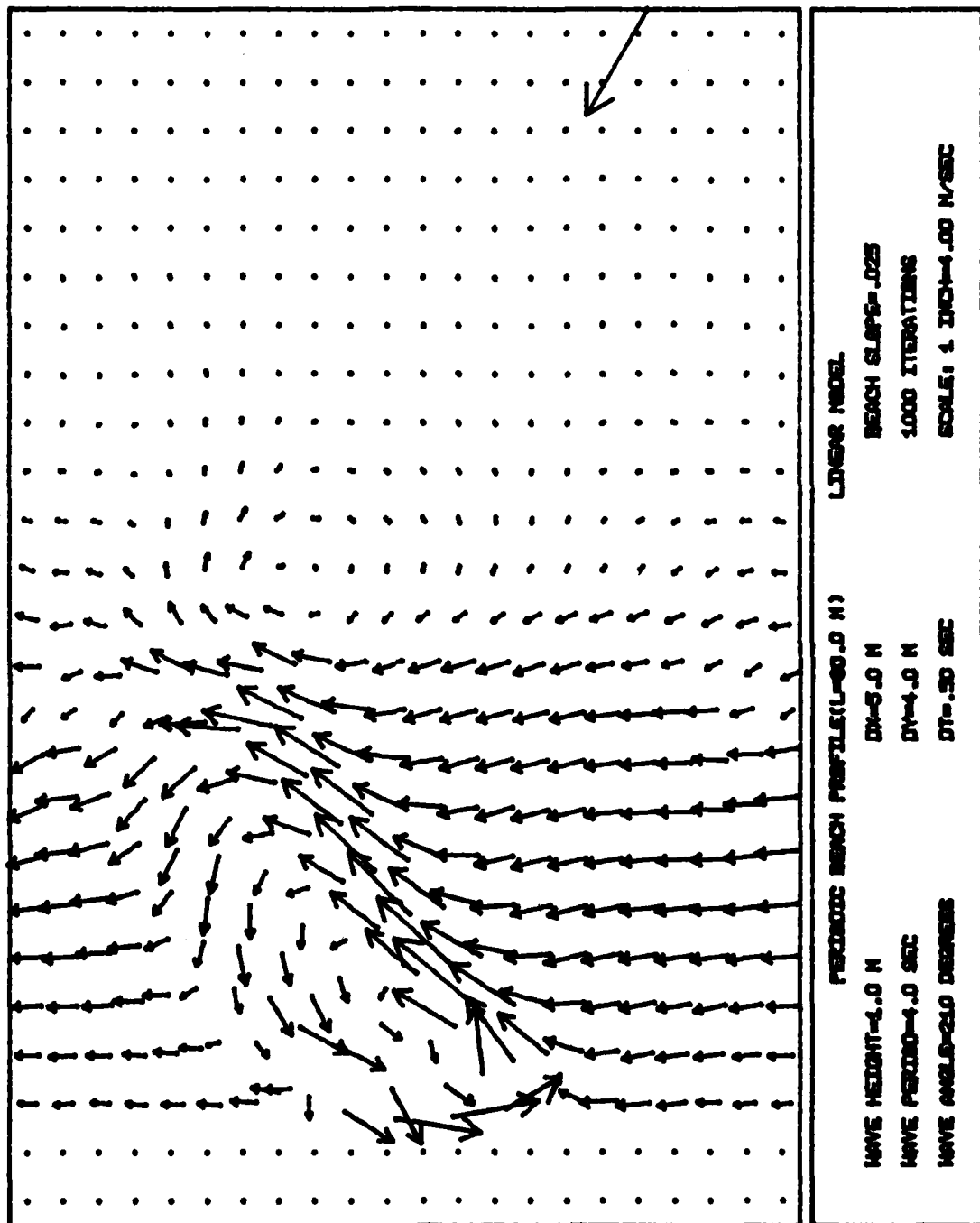


Figure 19 Current Vector Plot for the Model of Birkemeier and Dalrymple Run on the Periodic Bottom Topography

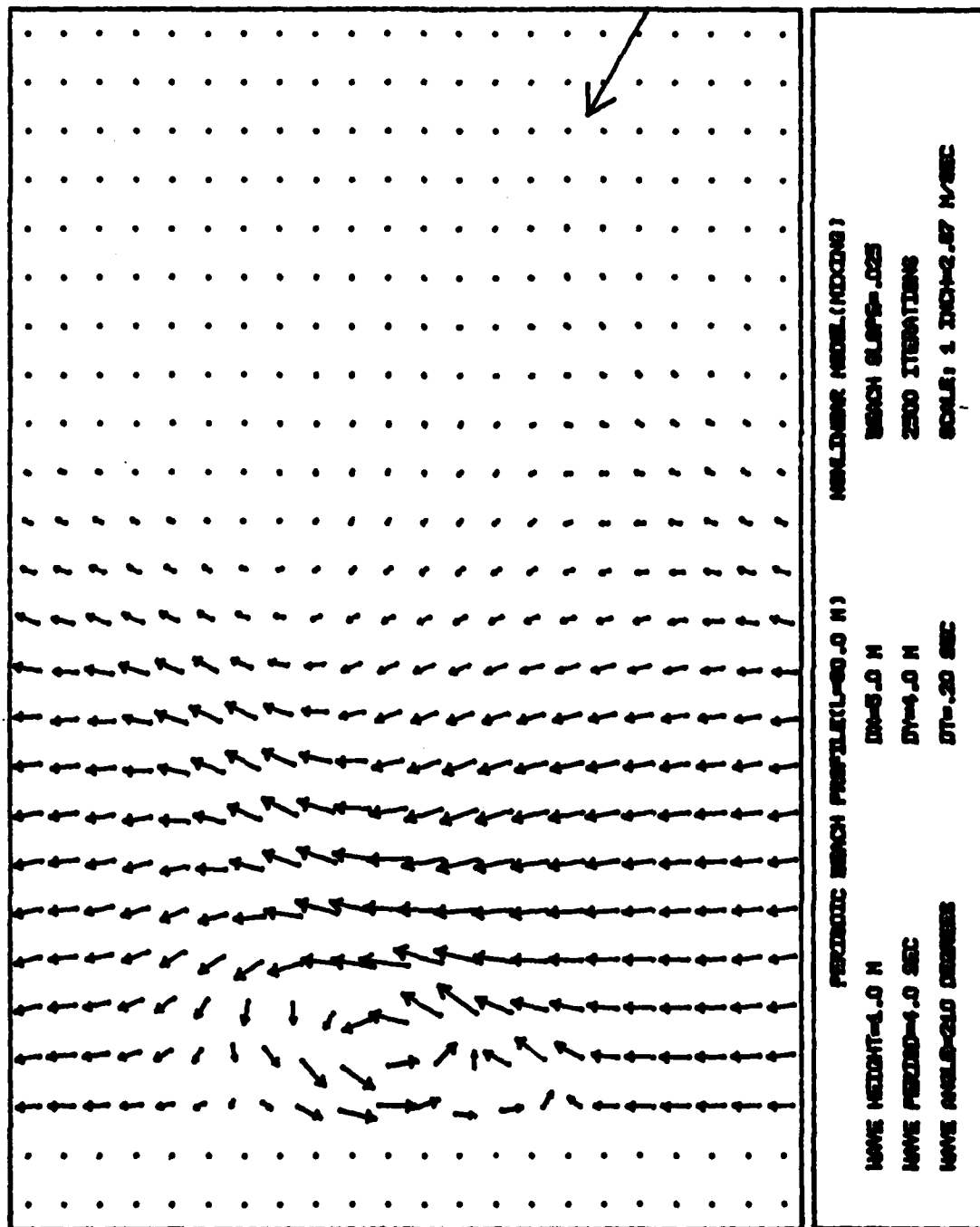


Figure 20 Current Vector Plot for the Present Model Including Mixing Run on the Periodic Bottom Topography. The arbitrary longshore mixing coefficient probably chosen as too large.

the linear model run is about 3.0 meters per second where, as in the non-linear model, it is about 0.8 meters per second. This large discrepancy is due to the inclusion of mixing in the non-linear model. The mixing tends to spread the rip out and decrease its offshore velocity components thus causing the rip to turn more in the longshore direction as shown in Figure 20. The effects of the convective acceleration terms are not clearly visible because it seems as though the form of the rip itself is governed primarily by horizontal mixing.

INTERSECTING WAVES APPLICATION

The final application of the model was to the case of intersecting wave trains of the same frequency on a plane beach which Dalrymple (1975) showed could generate rip currents. The purpose of this application was to investigate the effect of the convective acceleration terms in the model. The following derivation closely follows the work of Dalrymple.

Given two intersecting wave trains A and B with amplitudes a and b and a common frequency, σ , in terms of the coordinate system shown in Figure 21, the free surface displacements for the two wave trains can be written as,

$$\eta_1 = a \cos(k \cos \alpha x + k \sin \alpha y + \sigma t)$$

$$\eta_2 = b \cos(k \cos \beta x + k \sin \beta y + \sigma t) \quad .$$

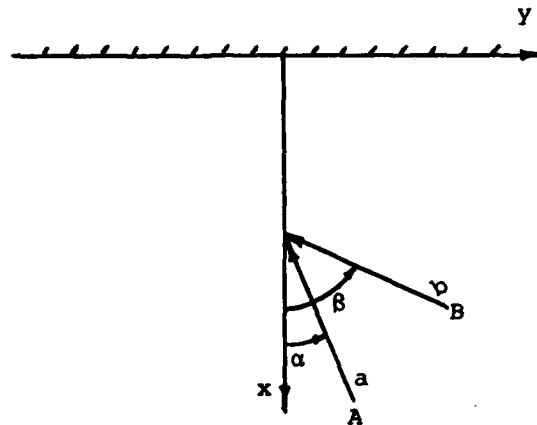


Figure 21 Definition Sketch for the Intersecting Waves Application

The total free surface $\eta_T = \eta_1 + \eta_2$ can then be written as,

$$\eta_T = 2a \cos \left\{ \frac{k}{2}(\cos \alpha + \cos \beta)x + \frac{k}{2}(\sin \alpha + \sin \beta)y + \sigma t \right\} \cdot$$

$$\cos \left\{ \frac{k}{2}(\cos \alpha - \cos \beta)x + \frac{k}{2}(\sin \alpha - \sin \beta)y \right\}$$

$$+ (b-a) \cos \{k \cos \beta x + k \sin \beta y + \sigma t\} \quad . \quad (44)$$

Using the linearized dynamic free surface boundary condition the velocity potential ϕ_T can be shown to equal,

$$\phi_T = \frac{2ag}{\sigma} \frac{\cosh k(h+z)}{\cosh kh} \sin \left\{ \frac{k}{2}(\cos \alpha + \cos \beta)x + \frac{k}{2}(\sin \alpha + \sin \beta)y + \sigma t \right\} \cdot$$

$$\cos \left\{ \frac{k}{2}(\cos \alpha - \cos \beta)x + \frac{k}{2}(\sin \alpha - \sin \beta)y \right\}$$

$$+ \frac{(b-a)g}{\sigma} \frac{\cosh k(h+z)}{\cosh kh} \sin(k \cos \beta x + k \sin \beta y + \sigma t) \quad .$$

From the velocity potential the total orbital velocities can be found from,

$$u = -\frac{\partial \phi}{\partial x}, \quad v = -\frac{\partial \phi}{\partial y}, \quad w = -\frac{\partial \phi}{\partial z}.$$

The radiation stresses, which are essentially the forcing terms, are defined as,

$$S_{xx} = \int_{-h}^0 \overline{\rho u^2} dz + \int_{-h}^{\eta} \overline{P} dz - \frac{1}{2} \rho g (h + \overline{\eta})^2 + \frac{1}{2} \rho g \overline{\eta^2}$$

$$S_{yy} = \int_{-h}^0 \overline{\rho v^2} dz + \int_{-h}^{\eta} \overline{P} dz - \frac{1}{2} \rho g (h + \overline{\eta})^2 + \frac{1}{2} \rho g \overline{\eta^2}$$

$$S_{xy} = \int_{-h}^0 \overline{\rho uv} dz$$

where

$$\overline{P} = \rho g (\overline{\eta} - z) + \frac{\partial}{\partial x} \int_z^0 \overline{\rho uw} dz + \frac{\partial}{\partial y} \int_z^0 \overline{\rho vw} dz - \overline{\rho w^2}.$$

Through tedious calculations the radiation stresses are found to be,

$$S_{xx} = \frac{\rho g}{4 \sinh 2kh} \left[a^2 \cos^2 \alpha + b^2 \cos^2 \beta + 2ab \cos \alpha \cos \beta \cos \{2 \textcircled{2}\} \right] \cdot \{2kh + \sinh 2kh\}$$

$$- \frac{\rho g ab}{8 \sinh 2kh} (\cos \beta - \cos \alpha)^2 \cos \{2 \textcircled{2}\} \cdot \{2kh \cosh 2kh - \sinh 2kh\}$$

$$- \frac{\rho g ab}{8 \sinh 2kh} (\sin \alpha - \sin \beta)^2 \cos \{2 \textcircled{2}\} \cdot \{2kh \cosh 2kh - \sinh 2kh\}$$

$$- \frac{\rho g}{4 \sinh 2kh} \left[a^2 + b^2 + 2ab \cos \{2(2)\} \right] \cdot \{\sinh 2kh - 2kh\}$$

$$+ \rho g ab \cos^2 (2) + \frac{1}{4} \rho g (b-a)^2$$

$$S_{yy} = \frac{\rho g}{4 \sinh 2kh} \left[a^2 \sin^2 \alpha + b^2 \sin^2 \beta + 2ab \sin \alpha \sin \beta \cos \{2(2)\} \right] \cdot \{2kh + \sinh 2kh\}$$

$$- \frac{\rho g ab}{8 \sinh 2kh} (\cos \beta - \cos \alpha)^2 \cos \{2(2)\} \cdot \{2kh \cosh 2kh - \sinh 2kh\}$$

$$- \frac{\rho g ab}{8 \sinh 2kh} (\sin \alpha - \sin \beta)^2 \cos \{2(2)\} \cdot \{2kh \cosh 2kh - \sinh 2kh\}$$

$$- \frac{\rho g}{4 \sinh 2kh} \left[a^2 + b^2 + 2ab \cos \{2(2)\} \right] \cdot \{\sinh 2kh - 2kh\}$$

$$+ \rho g ab \cos^2 (2) + \frac{1}{4} \rho g (b-a)^2$$

$$S_{xy} = \frac{\rho g}{4 \sinh 2kh} \left[a^2 \sin \alpha \cos \alpha + b^2 \cos \beta \sin \beta + ab \cos \{2(2)\} \sin(\alpha + \beta) \right] \cdot$$

$$\{2kh + \sinh 2kh\}$$

where the expression "(2)" is defined as,

$$(2) \equiv \frac{k}{2} (\cos \alpha - \cos \beta) x + \frac{k}{2} (\sin \alpha - \sin \beta) y$$

The time independent mean free surface displacement, $\bar{\eta}$,
is defined by

$$\bar{\eta} \equiv - \frac{1}{2g} \overline{\{u^2 + v^2 + w^2\}}_{z=0}$$

where "—" denotes the time average over one wave period.

Substituting the expressions for the velocity components u , v , and w from the velocity potential ϕ_T , $\bar{\eta}$ can be written as,

$$\bar{\eta} = \frac{-k}{2\sinh 2kh} \left[\overline{a^2 + b^2 + 2ab\cos\{2(2)\}} \cdot (\cos(\alpha - \beta) \cosh^2 kh - \sinh^2 kh) \right] \quad (45)$$

where "(2)" is the same quantity defined previously. Notice that the mean free surface displacement is modulated in the x and y directions by,

$$\cos\{k(\cos\alpha - \cos\beta)x + k(\sin\alpha - \sin\beta)y\} \quad .$$

Using Snell's Law which says,

$$k_o \sin \alpha_o = k \sin \alpha \quad \text{and} \quad k_o \sin \beta_o = k \sin \beta$$

and using the fact that $k_o \equiv \frac{2\pi}{L_o}$, where "o" denotes deep water values for the wave length, L , and the wave angles, α and β , we see that there is a periodicity of the mean displacement in the longshore direction with a periodic spacing, ℓ , given by,

$$\ell = \frac{L_o}{\sin \alpha_o - \sin \beta_o}$$

This periodicity in water level and wave height causes water to be driven from regions of high mean water level displacement to regions of lower displacement resulting in the formation of circulation cells.

In order to attempt to model this phenomena, certain simplifications to the model had to be made. Since the refraction and shoaling routines borrowed from the work of Noda, et al., could not treat more than one wave train, they were replaced with routines governed by Snell's Law neglecting wave-current interaction. Again a quadratic, "exact," bottom friction was used including velocities due to both mean currents and, this time, the two wave trains. In the momentum equations the advective acceleration terms were retained, horizontal mixing was neglected, and the radiation stresses were calculated using the results presented earlier in this section. A procedure for determining the wave heights for use in the radiation stresses and the bottom frictional stresses is given in Appendix B.

Three runs were made using different combinations of wave heights and wave angles. The remainder of the input data for all three runs, however, was the same and is given as follows. The waves were run on a plane beach with a slope of 0.025. The planform area of interest was comprised of 25 grids in the x direction with an Δx grid size of 5.0 meters, and 21 grids in the longshore direction

with a Δy grid size of 4.0 meters. The time step was chosen to be 0.2 seconds and the model was run for 1500 iterations for all three cases. A wave period of 7.159366 seconds was used which resulted in rip spacings of 80.0 meters. The bottom friction factor was set equal to 0.12 to allow the system to reach steady state after the 1500 iterations and to decrease the magnitude of the resultant currents.

The first case run used waves of equal heights and equal angles on either side of the beach normal. The deep water wave heights were 0.25 meters and the deep water angles were ± 30.0 degrees. For this case, referring to Equation (44), $a=b$ and $\alpha=-\beta$ resulting in a free surface displacement given by

$$\eta_T = 2a \cos(k_0 \sin \alpha_0 y) \cos(k \cos \alpha x + \sigma t) \quad .$$

This free surface describes a wave train moving in the $-x$ direction with a modulated wave height that is periodic in the longshore direction only. The periodicity in wave height is the driving mechanism producing the rip current perpendicular to the beach as shown in Figure 22. Note the constricted width of the rip current in relation to the width of the inflow region. This is a result of the convective acceleration terms. Also note the weak rip head where the currents diverge from the rip axis and return towards shore.

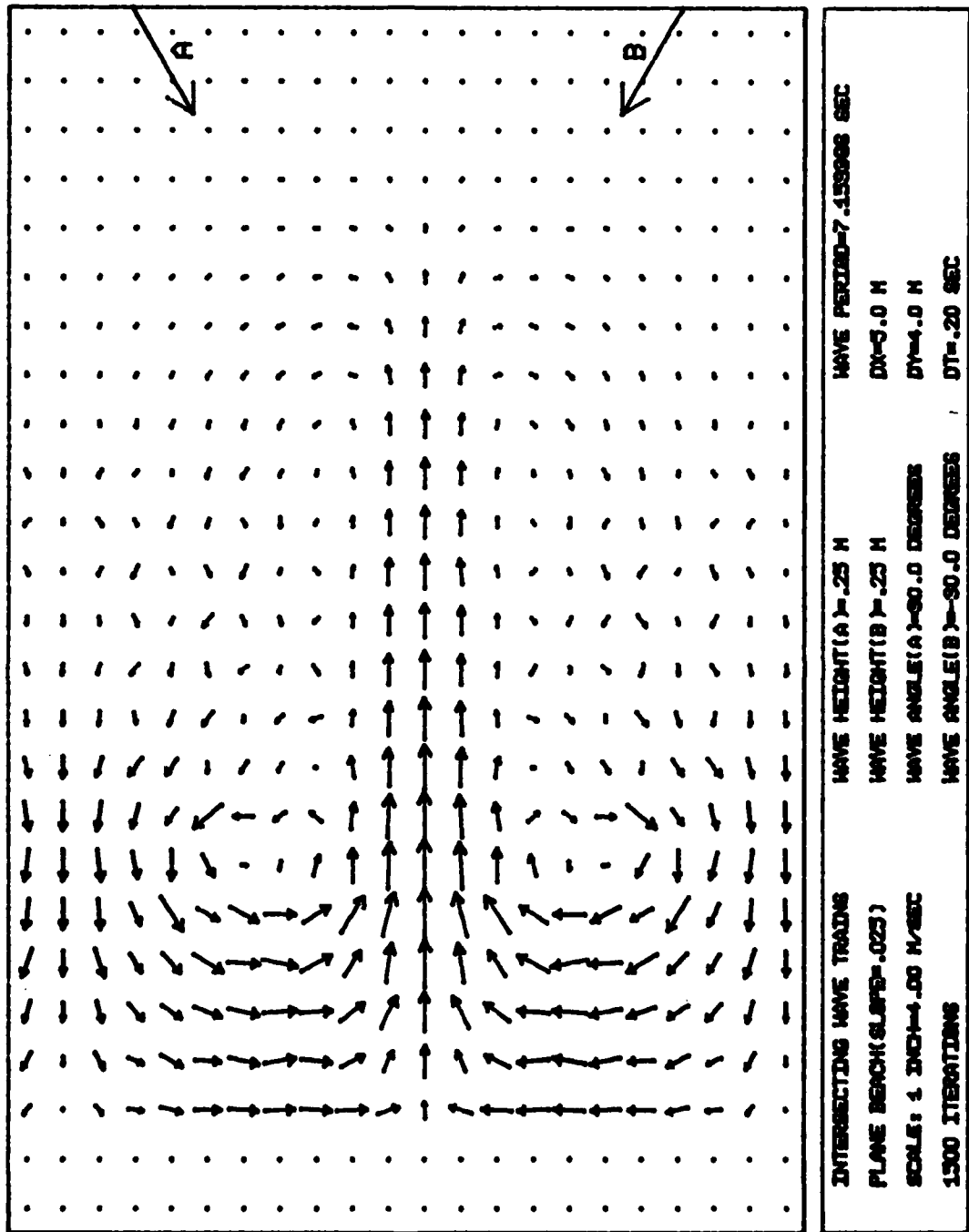


Figure 22 Current Vector Plot for a Rip Current Perpendicular to the Shoreline

In the second case the waves again were chosen to be of equal height (0.25 meters) but one wave approached normal to shore while the other approached at an angle of 60.0 degrees to the beach normal; i.e., $a=b$ but $\alpha \neq \beta$. The resulting free surface is modulated in both the x and y directions which should result in a rip current at an angle to the beach normal given by,

$$\theta = \tan^{-1} \left(\frac{\sin \alpha - \sin \beta}{\cos \alpha - \cos \beta} \right) .$$

For this case the angle should be about 30.0 degrees. The results are shown in Figure 23.

In the third case the waves, A and B, had different heights, 0.1 and 0.4 meters, and wave angles of 30.0 and -30.0 degrees, respectively. The resulting circulation pattern is shown in Figure 24. Note the meandering current with alternating regions of strong and weak longshore velocity along the beach. This circulation would lend itself well to the formation of rhythmic beach features. Looking at Equation (44), we see that there is a non-zero term,

$$(b-a)\cos\{k \cos \beta x + k \sin \beta y + \sigma t\}$$

which is a wave train at an angle to the beach normal with height $2(b-a)$. This wave is present in addition to the normal wave train with the modulated height from the first case causing a longshore current which is superimposed on the cellular circulation.

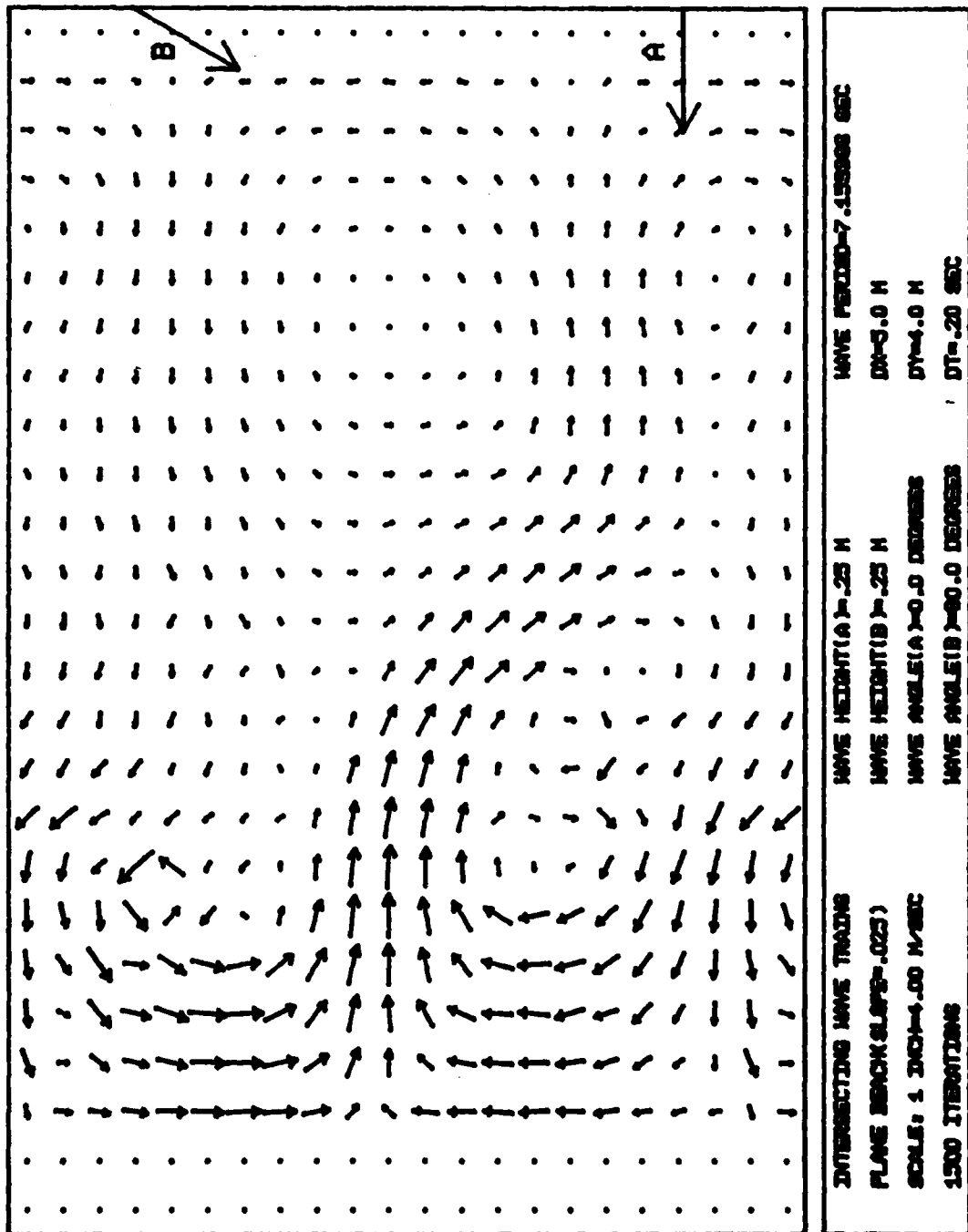


Figure 23 Current Vector Plot for a Rip Current at an Angle to the Shoreline. Note that in this case the offshore wall has influenced the flow.

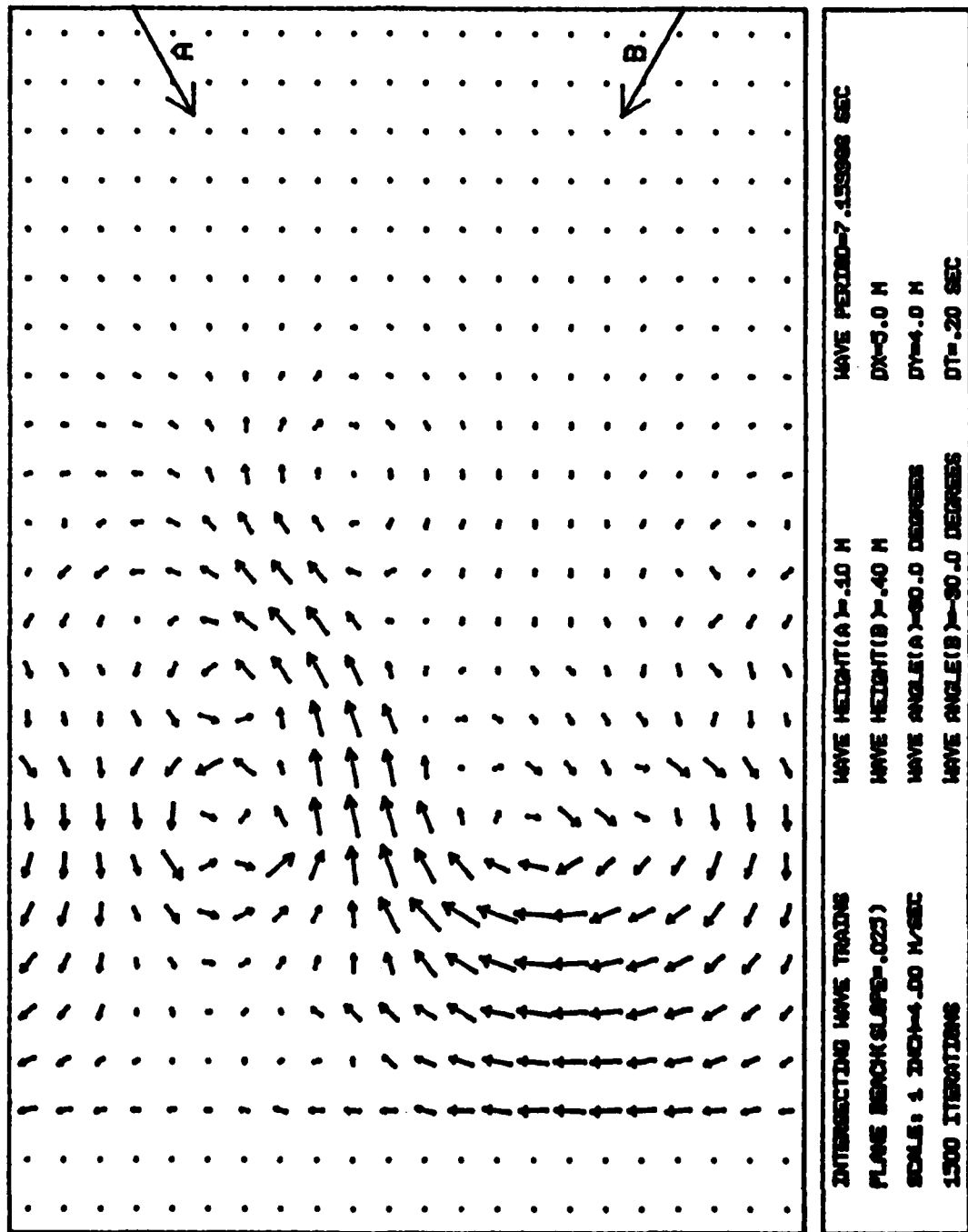


Figure 24 Current Vector Plot for the Meandering Circulation Pattern

CHAPTER VII CONCLUSIONS

A model that can accurately predict currents and wave transformations in the nearshore zone is a necessary step in attempting to predict actual changes to our coastlines. From the work done in this project and the results found, it appears that the inclusion of the convective acceleration terms and lateral mixing terms in the horizontal momentum equations have important effects on models used to predict nearshore circulation. The terms become especially significant in attempts to model circulation over irregular bottom topographies which include bars and channels.

There are still many aspects of the model that could be changed to make it even more complete. Among them are:

- (1) enable the model to handle more than one wave train within the wave-current interaction process,
- (2) include a better wave-current interaction scheme, especially in the surf zone, which could treat strong offshore flows that oppose the wave orbital velocities,
- (3) treat the continuity and momentum equations with an implicit scheme to avoid stability problems, or

- (4) obtain a better knowledge of the stability of the present model as a function of various parameters, and
- (5) create the ability to handle a variable grid size so that special regions of interest could be investigated in more detail.

In its present form the model is a very powerful tool yet continual improvements are needed to maintain its usefulness.

APPENDIX A
PERIODIC BOTTOM TOPOGRAPHY

The periodic bottom profile used in the model was developed by Noda, et al. (1974). The depths are given by

$$h = mx \left[1 + A \exp\left\{-3\left(\frac{x}{20}\right)^{1/3}\right\} \sin^{10} \frac{\pi}{\lambda} (y - x \tan \beta) \right]$$

where m = beach slope = .025

x, y are the coordinates of the depth location

λ = length of periodic beach = 80 meters

A = amplitude of bottom variation = 20

β = angle of rip channel to beach normal = 30 degrees.

The grid spacing was chosen to 5.0 and 4.0 meters in the x and y directions respectively. There were 25 and 21 grids in the x and y directions. The last grid row and the "dry" grid rows were made planar with the slope being .025.

APPENDIX B

DETERMINATION OF WAVE HEIGHTS FOR THE CASE OF INTERSECTING WAVES

Given the two wave trains

$$\eta_1 = a \cos(k \cos \alpha x + k \sin \alpha y + \sigma t)$$

$$\eta_2 = b \cos(k \cos \beta x + k \sin \beta y + \sigma t)$$

The total free surface $\eta_T = \eta_1 + \eta_2$ can be written as,

$$\eta_T = a \cos(\epsilon + \sigma t) + b \cos(\delta + \sigma t)$$

where ϵ and δ are phase functions. Expanding the expression for η_T and rearranging,

$$\eta_T = \cos \sigma t \{a \cos \epsilon + b \cos \delta\} - \sin \sigma t \{a \sin \epsilon + b \sin \delta\}$$

Defining $D \cos \theta \equiv a \cos \epsilon + b \cos \delta$

and $D \sin \theta \equiv a \sin \epsilon + b \sin \delta$

η_T becomes

$$\eta_T = D \cos(\sigma t + \theta)$$

where $D = \sqrt{(a \cos \epsilon + b \cos \delta)^2 + (a \sin \epsilon + b \sin \delta)^2}$.

Therefore, the total wave height due to the intersecting waves is
 2D. Substituting in the expressions for ϵ and δ , the total wave height can be written,

$$H_T = 2.0 \sqrt{a^2 + b^2 + 2ab \cos [k(\cos \alpha - \cos \beta)x + k(\sin \alpha - \sin \beta)y]} \quad (46)$$

The amplitudes a and b are given by the expressions

$$a = \frac{1}{2} H_A \kappa_{r_A} \kappa_{s_A} \quad (47)$$

$$b = \frac{1}{2} H_B \kappa_{r_B} \kappa_{s_B} \quad (48)$$

where κ_r and κ_s are the refraction and shoaling coefficients derived using Snell's Law.

To determine if breaking occurs, this total wave height is compared to a limiting breaker height of κh , here κ is a breaking coefficient chosen as 0.78. If the total wave height exceeded the value given by the breaking criterion, that value of κh was substituted into Equation (46) for H_T . A parameter β was defined such that $b \equiv \beta a$. This result was substituted into Equation (46) for b . The equation was then solved for a which gave b . The wave heights in the surf zone were then found using Equations (47) and (48).

REFERENCES

- Allender, J.H., Ditmars, J.D., Harrison, W. and Paddock, R.A., "Comparison of Model and Observed Nearshore Circulation," Proceedings of the 16th International Conference on Coastal Engineering, Hamburg, 1978.
- Birkemeier, W.A. and Dalrymple, R.A., "Nearshore Water Circulation Induced by Wind and Waves," Proc. of the Symposium on Modeling Technique, ASCE, 1975, pp. 1062-1081. Also, "Numerical Models for the Prediction of Wave Set-Up and Nearshore Circulation", ONR Tech. Rept. No. 1 and Ocean Eng. Rept. No. 3, Dept. of Civil Eng., Univ. of Del., Jan. 1976.
- Blumberg, A.F., "Numerical Tidal Model of Chesapeake Bay," Journal of the Hydraulics Division, ASCE, Vol. 103, No. HY1, January, 1977, pp. 1-9.
- Dalrymple, R.A., "A Mechanism for Rip Current Generation on an Open Coast," Journal of Geophysical Research, Vol. 80, 1975, pp. 3485-3487.
- Dalrymple, R.A., "Rip Currents and Their Genesis," Proc. of the 16th International Conference on Coastal Engineering, Hamburg, 1978.
- Holland, W.R. and Lin, L.B., "On the Generation of Mesoscale Eddies and Their Contribution to the Oceanic General Circulation. I. A Preliminary Numerical Experiment," Journal of Physical Oceanography, Vol. 5, October, 1975, pp. 642-657.
- Kurihara, Y., "On the Use of Implicit and Iterative Methods for Time Integration of the Wave Equation," Monthly Weather Review, Vol. 93, No. 1, January, 1965, pp. 33-46.
- Liu, P.L-F. and Dalrymple, R.A., "Bottom Frictional Stresses and Longshore Currents Due to Waves With Large Angles of Incidence," Sears Foundation: Journal of Marine Research, Vol. 36, No. 2, May, 1978, pp. 357-375.

Liu, P.L-F., and Lennon, G.P., "Finite Element Modeling of Nearshore Currents," Journal of the Waterway, Port, Coastal and Ocean Division, ASCE, Vol. 104, No. WW2, May, 1978, pp. 175-189.

Longuet-Higgins, M.S., "Longshore Currents Generated by Obliquely Incident Sea Waves, 1," Journal of Geophysical Research, Vol. 75, No. 33, November, 1970, pp. 6778-6789.

Longuet-Higgins, M.S., "Longshore Currents Generated by Obliquely Incident Sea Waves, 2," Journal of Geophysical Research, Vol. 75, No. 33, November, 1970, pp. 6790-6801.

Longuet-Higgins, M.S. and Stewart, R.W., "Radiation Stress and Mass Transport in Gravity Waves with Application to Surf Beats," Journal of Fluid Mechanics, Vol. 13, 1962, pp. 481-504.

Noda, E.K., Sonu, C.J., Rupert, V.C. and Collins, J.I., "Nearshore Circulations Under Sea Breeze Conditions and Wave-Current Interactions in the Surf Zone," Tetra Tech Report TC-149-4, February, 1974.

Pearce, B.R., "Numerical Calculation of the Response of Coastal Waters to Storm Systems with Application to Hurricane Camille of August 17-22, 1969," College of Engineering, University of Florida, Technical Report 12, August, 1972, 149 p.

Phillips, O.M., The Dynamics of the Upper Ocean, Cambridge University Press, 1969, pp. 45-48.

Roache, P.J., Computational Fluid Dynamics, Academic Press, 1972, pp. 60.

Wilson, W.S., "Seiche," in Encyclopedia of Oceanography, Reinhold Publishers, New York, 1966.